arXiv:nucl-ex/9606001v1 18 Jun 1996

Universality of Spectator Fragmentation at Relativistic Bombarding Energies

A. Schüttauf,(1) W.D. Kunze,(2) A. Wörner,(2) M. Begemann-Blaich,(2) Th. Blaich,(3)
D.R. Bowman,(4)[a] R.J. Charity,(5) A. Cosmo,(6) A. Ferrero,(7)[b] C.K. Gelbke,(4)
C. Groß,(2) W.C. Hsi,(4)[c] J. Hubele,(2) G. Immé,(8) I. Iori,(7) J. Kempter,(1) P. Kreutz,(1)
G.J. Kunde,(2)[d] V. Lindenstruth,(2)[e] M.A. Lisa,(4)[e] W.G. Lynch,(4) U. Lynen,(2)
M. Mang,(1) T. Möhlenkamp,(9) A. Moroni,(7) W.F.J. Müller,(2) M. Neumann,(1)
B. Ocker,(1) C.A. Ogilvie,(2)[f] G.F. Peaslee,(4)[g] J. Pochodzalla,(2)[h] G. Raciti,(8)
F. Rosenberger,(2) Th. Rubehn,(2)[e] H. Sann,(2) C. Schwarz,(2) W. Seidel,(9) V. Serfling,(1)
L.G. Sobotka,(5) J. Stroth,(2) L. Stuttge,(6) S. Tomasevic,(6) W. Trautmann,(2)
A. Trzcinski,(10) M.B. Tsang,(4) A. Tucholski,(10) G. Verde,(8) C.W. Williams,(4)
E. Zude,(2) and B. Zwieglinski(10)

(1) *Institut für Kernphysik, Universität Frankfurt, D-60486 Frankfurt, Germany*
(2) *Gesellschaft für Schwerionenforschung, D-64291 Darmstadt, Germany*
(3) *Institut für Kernchemie, Universität Mainz, D-55099 Mainz, Germany*
(4) *Department of Physics and Astronomy and National Superconducting Cyclotron Laboratory, Michigan State University, East Lansing, MI 48824, USA*
(5) *Department of Chemistry, Washington University, St. Louis, MO 63130, USA*
(6) *Centre de Recherches Nucléaires, F-67037 Strasbourg, France*
(7) *Istituto di Scienze Fisiche, Università degli Studi di Milano and I.N.F.N., I-20133 Milano, Italy*
(8) *Dipartimento di Fisica dell' Università and I.N.F.N., I-95129 Catania, Italy*
(9) *Forschungszentrum Rossendorf, D-01314 Dresden, Germany*
(10) *Soltan Institute for Nuclear Studies, 00-681 Warsaw, Hoza 69, Poland*

Corresponding author: W. Trautmann
GSI, D-64291 Darmstadt, Germany
e-mail: w.trautmann@gsi.de
Tel: x49-6159-71-2774, Fax: x49-6159-71-2989

ABSTRACT

Multi-fragment decays of ^{129}Xe, ^{197}Au, and ^{238}U projectiles in collisions with Be, C, Al, Cu, In, Au, and U targets at energies between $E/A = 400$ MeV and 1000 MeV have been studied with the ALADIN forward-spectrometer at SIS. By adding an array of 84 Si-CsI(Tl) telescopes the solid-angle coverage of the setup was extended to $\theta_{lab} = 16°$. This permitted the complete detection of fragments from the projectile-spectator source.

The dominant feature of the systematic set of data is the Z_{bound} universality that is obeyed by the fragment multiplicities and correlations. These observables are invariant with respect to the entrance channel if plotted as a function of Z_{bound}, where Z_{bound} is the sum of the atomic numbers Z_i of all projectile fragments with $Z_i \geq 2$. No significant dependence on the bombarding energy nor on the target mass is observed. The dependence of the fragment multiplicity on the projectile mass follows a linear scaling law.

The reasons for and the limits of the observed universality of spectator fragmentation are explored within the realm of the available data and with model studies. It is found that the universal properties should persist up to much higher bombarding energies than explored in this work and that they are consistent with universal features exhibited by the intranuclear cascade and statistical multifragmentation models.

Keywords: ^{129}Xe, ^{197}Au, ^{238}U projectiles, Be, C, Al, Cu, In, Au, U targets, $E/A = 400$, 600, 800, 1000 MeV; measured fragment cross sections, fragment charge, charge asymmetries and correlations; analysis using intranuclear cascade and statistical multifragmentation models.

PACS numbers: 25.70.Mn, 25.70.Pq, 25.75.-q

1 Introduction

The apparent absence of dynamical dependences is the perhaps most prominent feature of the multi-fragment decay of excited spectator nuclei. In the first experiments with the ALADIN spectrometer, performed with ^{197}Au beams of $E/A = 600$ MeV, it has manifested itself as an invariance of the observed patterns of projectile fragmentation with respect to the chosen target [1-3]. The mean number of projectile fragments produced as well as other observables characterizing the populated partition space were found to be the same for all targets, ranging from carbon to lead, if they were plotted as a function of Z_{bound}. The quantity Z_{bound} is defined as the sum of the atomic numbers Z_i of all projectile fragments with $Z_i \geq 2$. It represents the charge of the spectator system reduced by the number of hydrogen isotopes emitted during its decay.

It is easy to argue that Z_{bound} may, rather directly, reflect the energy transfer to the excited spectator system. The removal of nucleons in the initial excitation stage of the reaction and the release of hydrogen isotopes during the subsequent deexcitation are both correlated with the energy transfer. Larger energy transfers correspond to smaller values of Z_{bound}. The observed target invariance hence suggests that the energy transfer to the projectile spectator is the primary quantity governing its decay.

These characteristics represent, at least, an indication that statistical equilibrium is attained prior to the fragmentation stages of the reaction. In fact, statistical models were found to be quite successful in describing the measured fragment yields and correlations, provided that emission from an expanded breakup state was assumed [4-9]. Very recently, a near perfect description of the experimental charge correlations measured for the reaction ^{197}Au on Cu at $E/A = 600$ MeV, including their dispersions around the mean behavior, was achieved with the statistical multifragmentation model [10]. This comparison was made on an absolute scale, apart from an overall normalization constant which relates the number of model events to the measured cross section.

Intriguingly, the fragment-charge correlations from these first experiments were also reproduced to high accuracy with a variety of other models, such as site-bond-percolation [3], classical-cluster formation [11], fragmentation-inactivation binary [12], and restructuredaggregation models [13]. Some of these models are of a predominantly mathematical nature, have very few parameters, and do not contain any of the nuclear physics input on which the statistical models are based. Some exhibit critical behavior in the limit of an infinite number of constituents. It will be an interesting task to identify the underlying symmetries, apparently common to all of these models, and to study their relation to the universal properties of the fragment decay of excited nuclei [14].

The question of equilibration in the multi-fragment decay of excited spectator systems is of highest interest. Multifragmentation has been considered a manifestation of the liquid-gas phase transition in finite systems. The pursuit of this challenging problem (see, e.g. [15-17] and references given therein) will profit from the study of equilibrated systems that may be characterized by a few global variables such as mass, excitation energy, and temperature. The correlation of energy transfer and Z_{bound} opens the possibility to experimentally control the former quantity by selecting on the latter [17].

The present work was performed in order to further establish the validity of the observed universality and to search for its possible limits. The multi-fragment decay of heavy projectiles was explored over a wider range of projectiles and targets and within the regime of relativistic bombarding energies between 400 and 1000 MeV per nucleon. For these new experiments, the ALADIN spectrometer [2] has been upgraded by installing a new tracking detector TP-MUSIC III, by enlarging the time-of-flight wall behind it, and by mounting a new Si-CsI(Tl) hodoscope which provided good coverage of the solid-angle adjacent to the entrance of the spectrometer. In the data analysis, a consistent definition of the projectile-spectator source was adopted prior to comparing results from different reactions.

It was found that, within the realm of the present investigation, the universality of spectator fragmentation holds to very high accuracy. This includes the fragmentation of different projectiles if a linear scaling in proportion to their masses is applied to the data. In the following sections the experimental method and the obtained results will be presented in detail. The subsequent discussion will include comparisons to other data, some taken at much higher bombarding energies, and a search for related universal features within the intranuclear cascade and statistical multifragmentation models.

2 Experimental method

The experiments were performed at the heavy-ion synchrotron SIS of the GSI Darmstadt. Beams of ^{129}Xe at $E/A = 600$ MeV incident energy, of ^{197}Au at $E/A = 400$, 600, 800, and 1000 MeV, and of ^{238}U at $E/A = 600$ and 1000 MeV were used. Their intensities were of the order of a few thousand particles per second over spill lengths of several seconds. The areal densities of the targets made from Be, C, Al, Cu, In, Au and U were 190, 200, 390, 420, 800, 480, and 480 mg/cm^2, respectively, and corresponded to interaction probabilities between $\approx 0.7\%$ and 3.9%. Complete sets of targets were bombarded with the ^{197}Au beams (Be through Au) and with the ^{238}U beams (Be through U) at energies $E/A = 600$ and 1000 MeV. Only selected targets were used with the ^{129}Xe beam and with the ^{197}Au beams of $E/A = 400$ and 800 MeV.

A schematic layout of the experimental setup is shown in fig. 1. For each beam particle, its arrival time and its position in the plane perpendicular to the beam direction were measured upstream of the target with two thin plastic scintillators. Their effective thicknesses were 110 μm and 50 μm. The geometric acceptance of the spectrometer of $\theta_{lab} \approx \pm 9.2^\circ$ horizontally and $\pm 4.3^\circ$ vertically was matched by the dimensions of the new multiple sampling ionization chamber TP-MUSIC III and by the extended time-of-flight (TOF) wall. At $E/A = 1000$ MeV, these detector systems permitted the detection of close to 100% of all projectile fragments with atomic number $Z \geq 2$. At the lower bombarding energies, the angular distributions of some lighter fragments extended beyond the acceptance of the spectrometer but stayed within the acceptance of the Si-CsI(Tl) hodoscope array that surrounded the entrance to the field gap of the magnet. For very light fragments, up to $Z \approx 4$, the emissions from the projectile and mid-rapidity sources are not clearly separated in momentum space. Therefore, a consistent definition of the projectile spectator source had to be adopted for the data analysis. This will be described in section 3.1.

The atomic numbers Z and the velocities of nuclear fragments were determined with the TOF wall, located at the end of the ALADIN spectrometer and extending over 2.4 m in horizontal and 1.0 m in vertical directions. It consisted of two layers of vertically mounted scintillator strips of 2.5 cm width and 1.0 cm thickness, viewed by photomultiplier tubes at

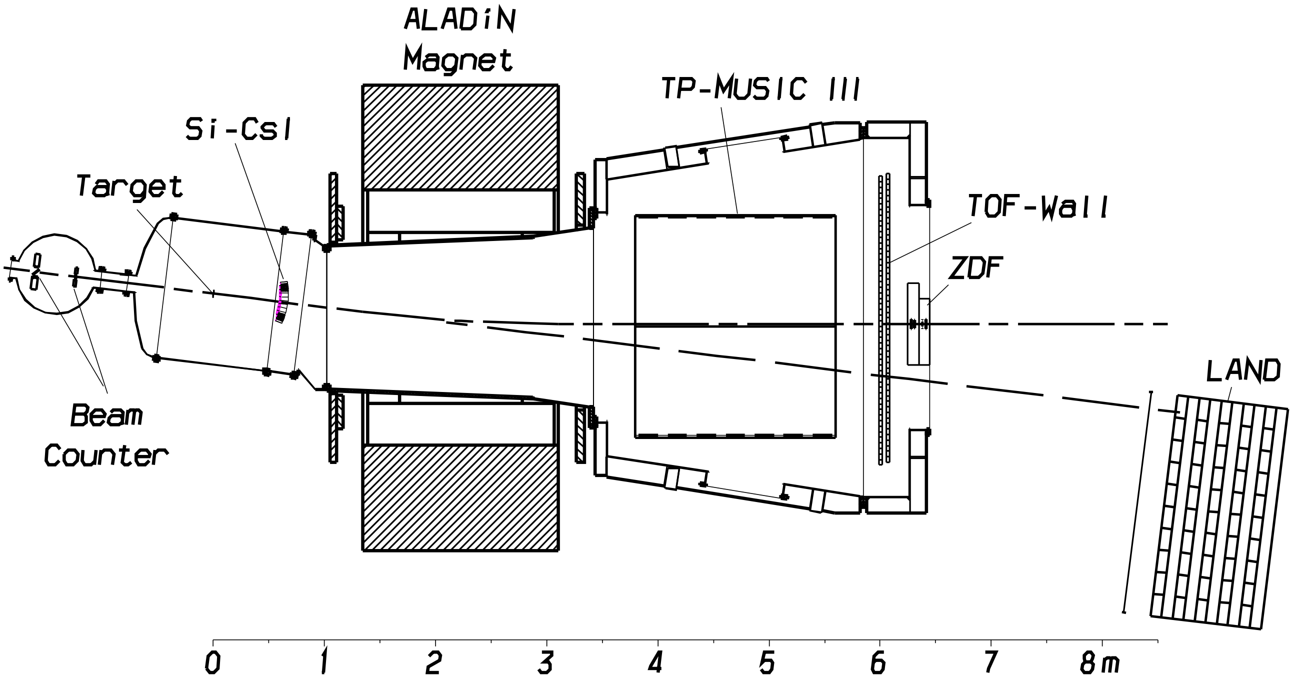

Figure 1: *Cross sectional view of the ALADIN facility. The beam enters from the left and is monitored by two beam detectors before reaching the target. Projectile fragments entering into the acceptance of the magnet are tracked and identified in the TP-MUSIC III detector and in the time-of-flight (TOF) wall. The Central Plastic detector covers the hole in the TOF wall at the exit for the beam. Fragments and particles emitted in forward directions outside the magnet acceptance and up to* $\theta_{lab} = 16^\circ$ *are detected in the Si-CsI array. Neutrons emitted in directions close to 0° are detected with the large-area neutron detector (LAND). The dashed line indicates the direction of the incident beam. The dash-dotted line represents the trajectory of beam particles after they were deflected by an angle of 7.3°. The Miniball/Miniwall detector system used at* $E/A = 400$ *MeV is not shown.*

both ends [2]. The two layers were offset by half a width with respect to each other. The primary beam was directed through a hole of 4.8 x 6.0 cm^2 cut into the middle sections of the central slats. The upper and lower halves of these central slats were optically connected by a hollow light guide built from aluminized mylar foil. The discriminator threshold was set to be below $Z = 2$ particles. For the time-of-flight calibration, primary beams of reduced intensity were swept across the wall with the Aladin magnet. By inducing fragmentation reactions in a thick aluminum target positioned immediately in front of the wall the response to fragments of different Z was determined. A resolution of about 400 ps and 180 ps (FWHM) for fragments of $Z = 2$ and $Z \approx Z_P$, respectively, was achieved (Z_P denotes the atomic number of the projectile). These values include the systematic uncertainty of the calibration. The intrinsic time-of-flight resolution measured for beam particles was 120 ps.

The algorithm used for fragment identification in the TOF-wall analysis took into account that fragments may pass into the narrow gap between adjacent slats in one of the two layers of the wall and that heavy fragments are accompanied by a considerable number of δ-rays. The identification spectrum for the TOF-wall detectors was obtained by projecting along the ridges of constant Z in two-dimensional maps of the measured pulse height versus time of flight. Elements with $Z \leq 15$ were resolved individually. For heavier fragments the resolution assumed values of up to $\Delta Z \approx 1.5$ (FWHM). For this analysis, the TP-MUSIC III detector, capable of identifying the individual elements for $Z \geq 8$ with a resolution between $\Delta Z \approx 0.8$ (FWHM, $Z \approx 20$) and $\Delta Z \approx 0.4$ ($Z \approx 60$), served to calibrate the charge response of the TOF wall. The main purpose of the TP-MUSIC, in these experiments, was to provide the tracking information for other analyses that involved the fragment momenta. The dynamic range for tracking had been extended down to $Z = 2$ by using gas amplification over part of the length of the detector which permitted the measurement of isotopic yield ratios of light fragments [17]. The high charge resolution of the TP-MUSIC was essential for the analysis of fission decays in experiments with the uranium beams [18-20].

The Z resolution achieved with the two detector systems after off-line calibration is demonstrated in fig. 2. A good separation of $Z = 2$ and 3 fragments was crucial for the

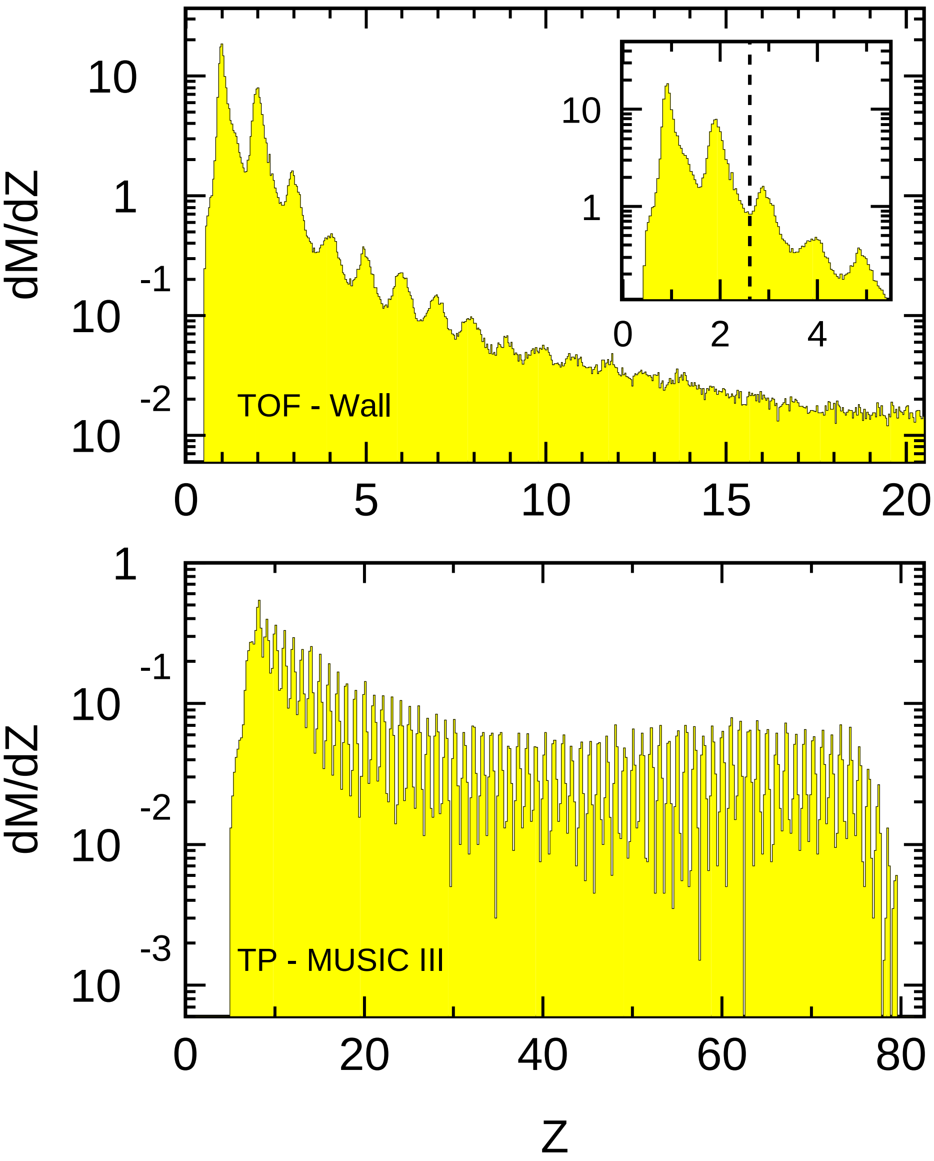

Figure 2: *Z-identification spectra measured with the TOF wall (top) and the TP-MUSIC (bottom) for the reaction* ^{197}Au *on* ^{197}Au *at* $E/A = 600$ *MeV. The Z information from the TP-MUSIC was used to calibrate the response of the TOF wall in the region* $Z > 15$*. Note that the element yield at* $Z > 65$ *is affected by the experimental trigger.*
Insert: Low-Z part of the TOF-wall spectrum. The dashed line indicates the equivalent sharp cut which was used for selecting fragments with $Z \geq 3$*.*

reliable determination of the multiplicity of intermediate-mass fragments with $Z \geq 3$. Therefore, the $Z = 2$ and 3 distributions in the Z-identification spectrum were fitted individually and, after evaluation of their overlapping tails, the position of an equivalent sharp Z-cut was determined (fig. 2, insert).

The Si-CsI(Tl) hodoscope was positioned 60 cm downstream from the target and covered the solid angle surrounding the spectrometer acceptance up to angles $\theta_{lab} \approx 16°$. Its 84 telescope modules were mounted in close geometry. Each detector consisted of a 300-μm Si detector followed by a 6-cm long CsI(Tl) detector which was viewed by a 1-cm^2 photodiode from the end face. The active area of each detector was 30 x 30 mm^2; the solid-angle coverage of the hodoscope with respect to the subtended solid angle, i.e. not counting the central rectangular opening, amounted to 85%. Light fragments with approximately beam velocity were not stopped by the telescopes. For these particles, the identification had to be based on the two-fold measurement of their energy loss. The peaks caused by fast hydrogen, helium, and lithium ions are clearly visible in the identification spectrum obtained from a weighted sum of the two ΔE measurements with the hodoscope detectors (fig. 3).

For the actual analysis, gates were set in the two-dimensional ΔE_1 versus ΔE_2 spectra which permitted the identification of stopped fragments and a more efficient suppression of background. The yield of fragments with $Z \geq 3$, selected in this way, is given by the dark-shaded distribution shown in fig. 3. The insert shows the distribution of these fragments, mostly lithium, across the solid angle subtended by the hodoscope for the reaction ^{197}Au on ^{197}Au at $E/A = 600$ MeV. Each square represents a detector element, with its area being proportional to the number of detected fragments. The circle indicates the angular limit up to which fragments were considered as belonging to the spectator source at this incident energy (see section 3.1).

For the runs at 600, 800, and 1000 MeV per nucleon, a 5-mm thick central plastic detector with light-fiber readout was installed behind the central hole of the TOF wall. It served for the detection of the primary beam particles and of projectile fragments emitted along directions close to that of the beam, and for their identification according to the measured energy-loss signal. The large-area neutron detector LAND was positioned close

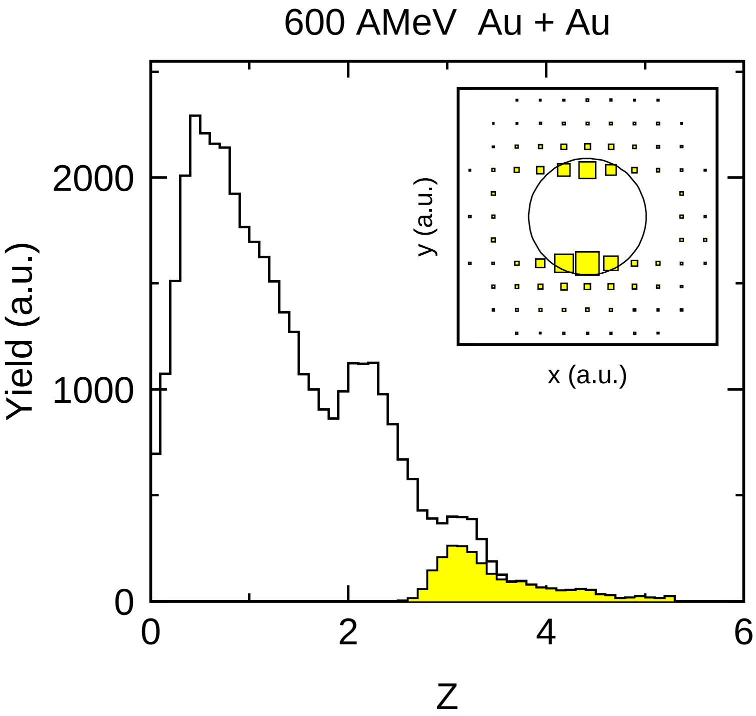

Figure 3: *Z-identification spectrum, obtained from a weighted sum of the two energy-loss measurements with the Si-CsI(Tl) telescopes of the hodoscope for the reaction* ^{197}Au *on* ^{197}Au *at* E/A = *600 MeV. Intermediate-mass fragments of* $Z \geq 3$*, as identified in the two-dimensional energy-loss spectrum, are represented by the dark-shaded distribution. Insert: Distribution of intermediate-mass fragments across the solid angle subtended by the hodoscope detectors. Each square represents a telescope module with its area being proportional to the detected fragment yield. The circle is meant to illustrate that six hodoscope detectors are within the angular limit of the spectator source at this incident energy.*

to zero degrees with respect to the incident beam direction and operated in a calorimetric mode. First results obtained from the measurement of coincident neutrons with LAND have been reported elsewhere [17, 21]. The experiment at 400 MeV per nucleon was performed with the Miniball/Miniwall [22] installed around the target. This detector system covered the angular range from $\theta_{lab} = 14.5°$ to $\theta_{lab} = 160°$ and, together with the Si-CsI(Tl) hodoscope, provided an efficient 4-π multi-particle detection capability. Results from the coincident detection of fragments from the target and projectile spectators and from the mid-rapidity source are given in ref. [23]. For the present study of the projectile spectator, the increased coverage of the mid-rapidity emission by the Miniball/Miniwall detectors permitted a good event selection according to multiplicity. This was particularly useful as the central plastic detector was not in operation at this energy. Peripheral events with a small apparent Z_{bound}, due to the escape of a heavy projectile residue through the central hole of the TOF wall, were identified by their small associated multiplicity.

The on-line trigger condition consisted of the logical product of the requirements of a beam particle in the start detector, no fragment with Z close to that of the beam in the central plastic detector or in the central part of the TOF wall, and the detection of at least one particle with the Si-CsI(Tl) hodoscope. It had the effect of suppressing the most peripheral interactions except those leading to binary fission. For the present study of multi-fragment production, the peripheral fission events which may have large cross sections, in particular for the case of ^{238}U projectiles [18], were suppressed off-line. In the experiment with the ^{197}Au beam of 400 MeV per nucleon, a beam particle in the start detector and a minimum of one particle detected with the Miniball/Miniwall or the Si-CsI(Tl) hodoscope were required. Scaled down events with less restrictive trigger conditions, including beam events triggered only by the beam detectors, were recorded for normalization.

Absolute cross sections were determined by normalizing the measured event rate with respect to the thickness of the target and the rate of incoming beam particles. The error of the normalization, dominated by the uncertainty of the areal density of the targets, is between 1% and 5%. The uncertainties of the measured fragment multiplicities and correlations will be discussed in section 3.3.

3 Experimental results

3.1 Spectator source

The ALADIN spectrometer has been designed for optimum acceptance of projectile fragments which are emitted in forward directions. However, the effect of forward focussing by the reaction kinematics is a function of the projectile velocity and changes with changing bombarding energy. We have therefore studied the extension of the projectile-spectator source in rapidity y and in transverse momentum p_t, both experimentally and with model calculations.

Rapidity spectra of light fragments detected with the TOF wall in the reaction ^{197}Au on ^{197}Au at $E/A = 1000$ MeV are shown in fig. 4. The distributions are concentrated around a rapidity value very close to the beam rapidity and become increasingly narrower with increasing mass of the fragment. The deviation of the most probable rapidity $y = 1.32$ of light fragments (full line in fig. 4) from the rapidity $y_P = 1.35$ of the beam, after it has passed through half of the Au target, is within the uncertainty of the absolute time-of-flight calibration. For the lighter fragments, the distributions are wider and extend into the mid-rapidity region. The widths and shapes of the distributions also depend on the impact parameter, as demonstrated for helium fragments in the two lower panels of fig. 4. Both the dispersion around the projectile rapidity and the relative intensity at mid-rapidity increase with increasing centrality.

The bump in the peripheral He spectrum, located at a rapidity y between 0.8 and 0.9, originates from mid-rapidity emission. This was confirmed by simulating the emission with two Maxwellian sources centered at projectile rapidity and at mid-rapidity. The restriction of the acceptance to forward angles causes the maximum of the observed mid-rapidity yield to appear at this somewhat larger rapidity. For this reason, the two sources can only be discerned in the peripheral collisions with lower emission temperatures. In more central collisions, the mid-rapidity source no longer produces an identifiable bump in the rapidity spectrum. Indications of a mid-rapidity source are only observed for light fragments up to $Z \approx 4$ (fig. 4, top), in agreement with the rapid drop of the element yields in central collisions at relativistic bombarding energies [24].

Guided by these observations, we chose a lower limit in rapidity of $y \geq 0.75 \cdot y_P$ where y_P is the projectile rapidity, so as to define the spectator source. This condition was applied to fragments detected with the TOF wall. For those detected with the hodoscope, for which an equivalent time-of-flight information does not exist, angular limits were set with the same purpose of selecting the spectator source. They are motivated and described below.

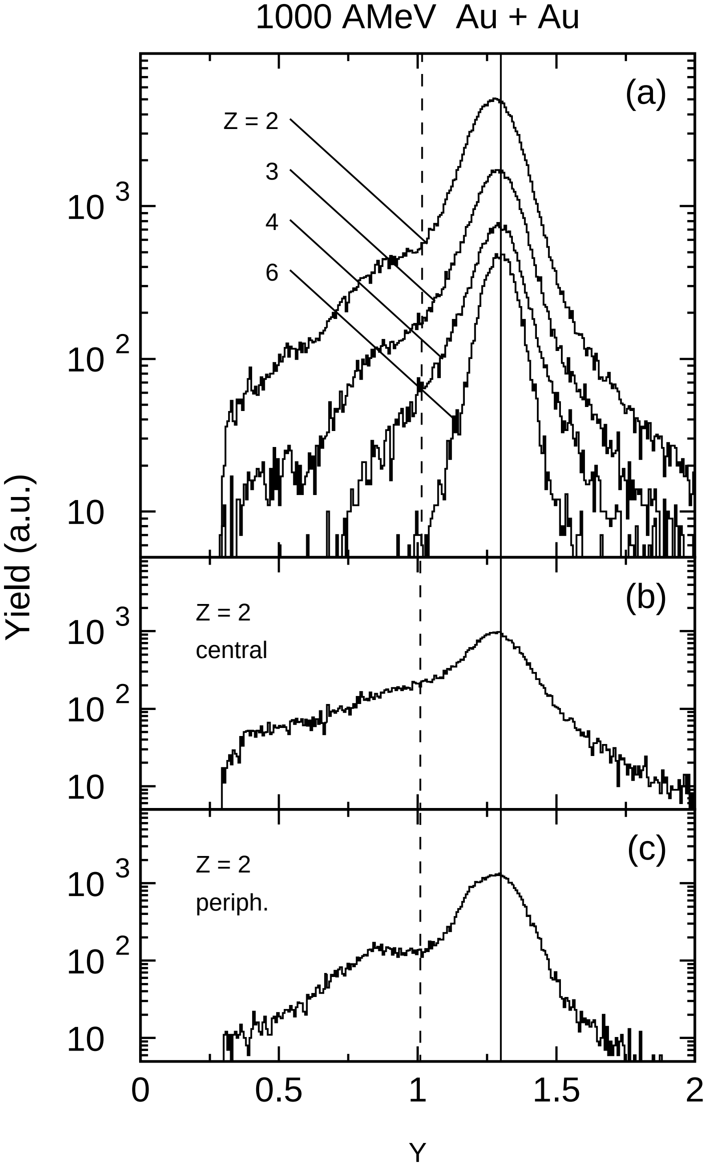

Figure 4: *(a): Rapidity spectra measured in the reaction* ^{197}Au *on* ^{197}Au *at* $E/A =$ *1000 MeV for fragments with* $Z = 2, 3, 4,$ *and 6. The solid and dashed lines indicate the measured most probable rapidity* $y = 1.32$ *of the light fragments and the condition* $y \geq 0.75 \cdot y_P$ *adopted for fragments from the projectile spectator, respectively.*
(b): Rapidity spectra of helium fragments, measured in central collisions ($Z_{bound} \leq 30$*) for the same reaction.*
(c): Same as (b) for peripheral collisions ($Z_{bound} \geq 50$*).*

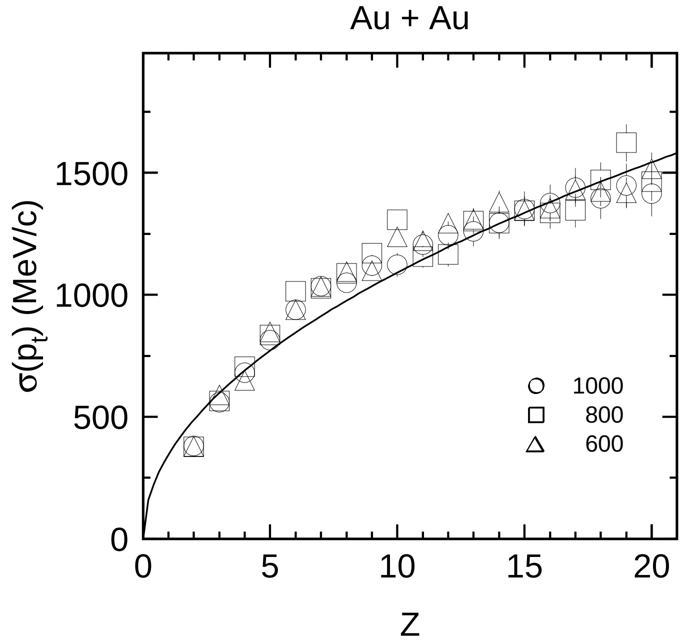

Figure 5: *Widths of the transverse-momentum distributions* $\sigma(p_t)$ *as a function of* Z *for the reactions* ^{197}Au *on* ^{197}Au *at* E/A *= 600, 800, and 1000 MeV and for 20* $\leq Z_{bound} \leq$ *60. The line is proportional to* $\sqrt{Z}$*.*

Transverse momentum distributions were constructed from the vertical position distributions of fragments measured with the TOF wall. The vertical coordinate is perpendicular to the bending plane of the magnet. In fig. 5 we show the widths

$$\sigma(p_t) \approx \sqrt{2} \cdot \sigma(r_y/L) \cdot A \cdot p_P/A_P \qquad (1)$$

as a function of Z for the reactions ^{197}Au on ^{197}Au at E/A = 600, 800, and 1000 MeV. Here r_y/L is the ratio of the vertical position r_y of a fragment to the length L of the flight path and $\sigma(r_y/L)$ is the width of the distribution as obtained by Gaussian fitting. The length L was approximated by using the nominal trajectory, starting at the target with θ_{lab} = 0°, to the particular slat of the TOF wall that was hit. A is the mass number assumed for fragments with a given Z, p_P and A_P are the momentum and the mass number of the projectile. We have used $A = 2 \cdot Z$ for $Z \leq 10$ and the EPAX parameterization [25] for heavier fragments.

The widths $\sigma(p_t)$ rise approximately in proportion to $\sqrt{Z}$, i.e. the mean transverse energies are independent of Z which is expected for emission from an equilibrated source (see section 3.5). It is, furthermore, evident that the transverse momentum distributions of the emitted projectile fragments do virtually not change with the bombarding energy. There are no indications of any dynamical contributions to the fragment velocities in the moving frame which could be related to the incident energy. Therefore, in order to select the spectator source, upper limits of the laboratory angle were imposed on the hodoscope data that were inversely proportional to the projectile momentum per nucleon. The same limits were used for all three projectiles because the dependence of the p_t distributions on the projectile mass was found to be insignificant for the light fragments.

At 1000 MeV per nucleon, the adopted angular limit coincides with the vertical acceptance of the ALADIN magnet of $\theta_{lab} = \pm 4.3°$. For the helium isotopes, this corresponds to the condition $|p_y| \leq 2\sigma(p_y)$ where $\sigma(p_y)$ is the width of the transverse momentum distribution in vertical direction. At the lower incident energies 800, 600, and 400 MeV per nucleon, the resulting angular limits are $\theta_{lab} = 5.0°$, $6.0°$, and $7.7°$, respectively. Consequently, the fragment yields detected with the corresponding central detectors of the Si-CsI(Tl) telescope array were counted as belonging to the projectile spectator. At 600 MeV per nucleon, this included six detectors, as illustrated in fig. 3 (insert). They contributed about 10% of the fragment yield at this energy, mostly very light fragments with $Z = 3$ and above.

3.2 Charge correlations for ^{197}Au + ^{197}Au

With the definitions of the spectator source in rapidity and angle, as given in the previous section, the fragmentation patterns in ^{197}Au on ^{197}Au collisions were studied. Figure 6 shows the correlation between the mean multiplicity of intermediate-mass fragments $\langle M_{IMF} \rangle$ and Z_{bound} for the four bombarding energies. Here intermediate-mass fragments (IMF's) were selected according to the definition $3 \leq Z \leq 30$. The familiar rise and fall of the fragment production is seen to be independent of the projectile energy within the experimental accuracy. The invariance with respect to the target, as observed earlier [1-

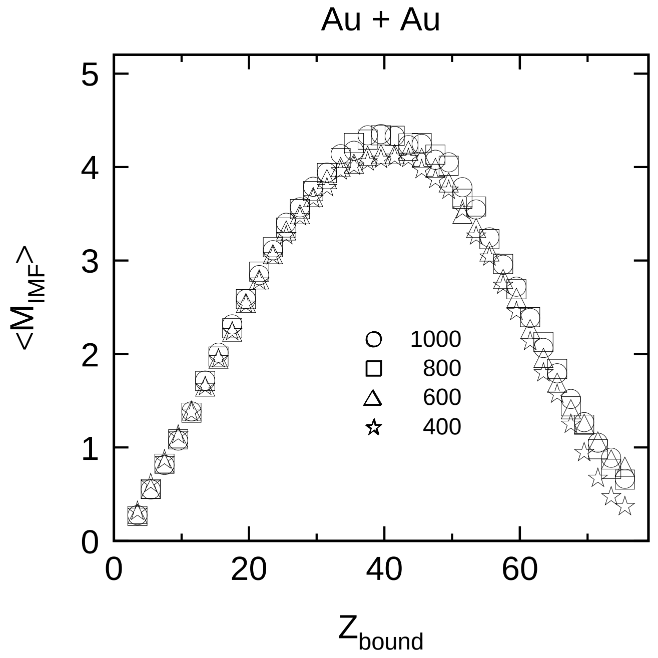

Figure 6: *Mean multiplicity of intermediate-mass fragments* $\langle M_{IMF} \rangle$ *as a function of* Z_{bound} *for the reaction* ^{197}Au *on* ^{197}Au *at* E/A = *400, 600, 800, and 1000 MeV.*

3] and discussed further in section 3.4, is thus complemented by an invariance over the range of bombarding energies studied in the present experiment. At $Z_{bound} \approx 40$ the mean multiplicity $\langle M_{IMF} \rangle$ reaches its maximum of 4 to 4.5. Due to the enlargement of the spectrometer acceptance and the chosen source definition, this value exceeds the one reported earlier [1-4] by one half to one unit. For the same reason, the position of the maximum is shifted to a slightly larger value of Z_{bound}.

The definition of the spectator source is most crucial for the multiplicities of the lightest projectile fragments such as helium, lithium, and beryllium nuclei. Heavier fragments are more strongly localized in velocity space (cf. figs. 4 and 5). Figure 7 shows the mean multiplicities $\langle M_Z \rangle$ for several light elements as a function of Z_{bound} for the incident energy 1000 MeV per nucleon. The present analysis yields a maximum of 4.5 helium nuclei near $Z_{bound} = 30$ whereas, with the acceptance of the TOF wall in the previous experiment at 600 MeV per nucleon, only about 3.5 helium nuclei were detected at the maximum [10].

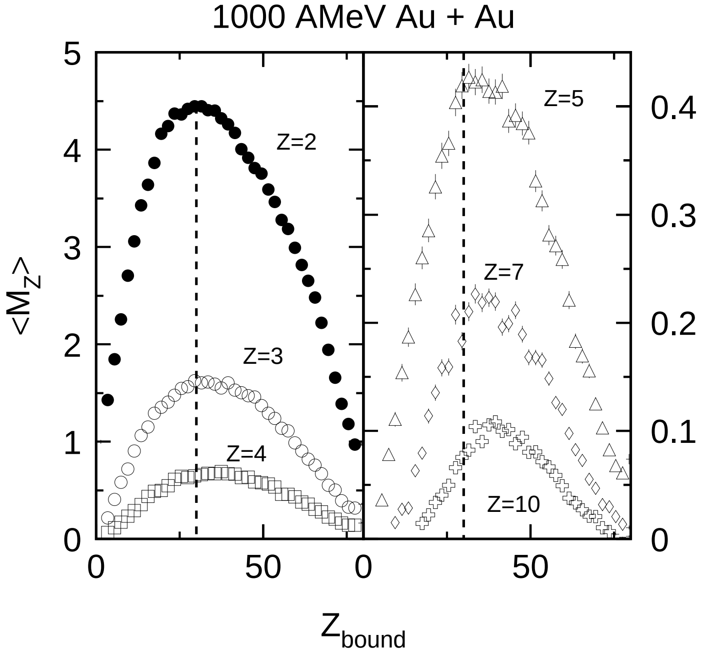

Figure 7: *Mean values of the multiplicities* $\langle M_Z \rangle$ *for selected elements as a function of* Z_{bound} *for the reaction* ^{197}Au *on* ^{197}Au *at* E/A *= 1000 MeV. The dashed lines mark the value* $Z_{bound} = 30$ *where* $\langle M_2 \rangle$ *assumes its maximum.*

Lithium is by far the most abundant element in the range of fragments with intermediate mass. Its maximum multiplicity is 1.6 at $Z_{bound} = 35$. With increasing Z the maxima of the multiplicity distributions continue to shift to larger values of Z_{bound}. For elements up to $Z = 10$ this is shown in fig. 7.

The invariance with respect to the bombarding energy also holds for other charge correlations that have been found useful to characterize the population of the partition space in the fragmentation process [3]. Six of these observables, as measured at the four bombarding energies, are given in fig. 8 as a function of Z_{bound}. They include the mean values of the maximum fragment charge Z_{max} of the event and of three asymmetry variables. The latter are the charge asymmetry $a_{12} = (Z_{max} - Z_2)/(Z_{max} + Z_2)$ between the two largest fragments, the charge asymmetry $a_{23} = (Z_2 - Z_3)/(Z_2 + Z_3)$ between the second and third

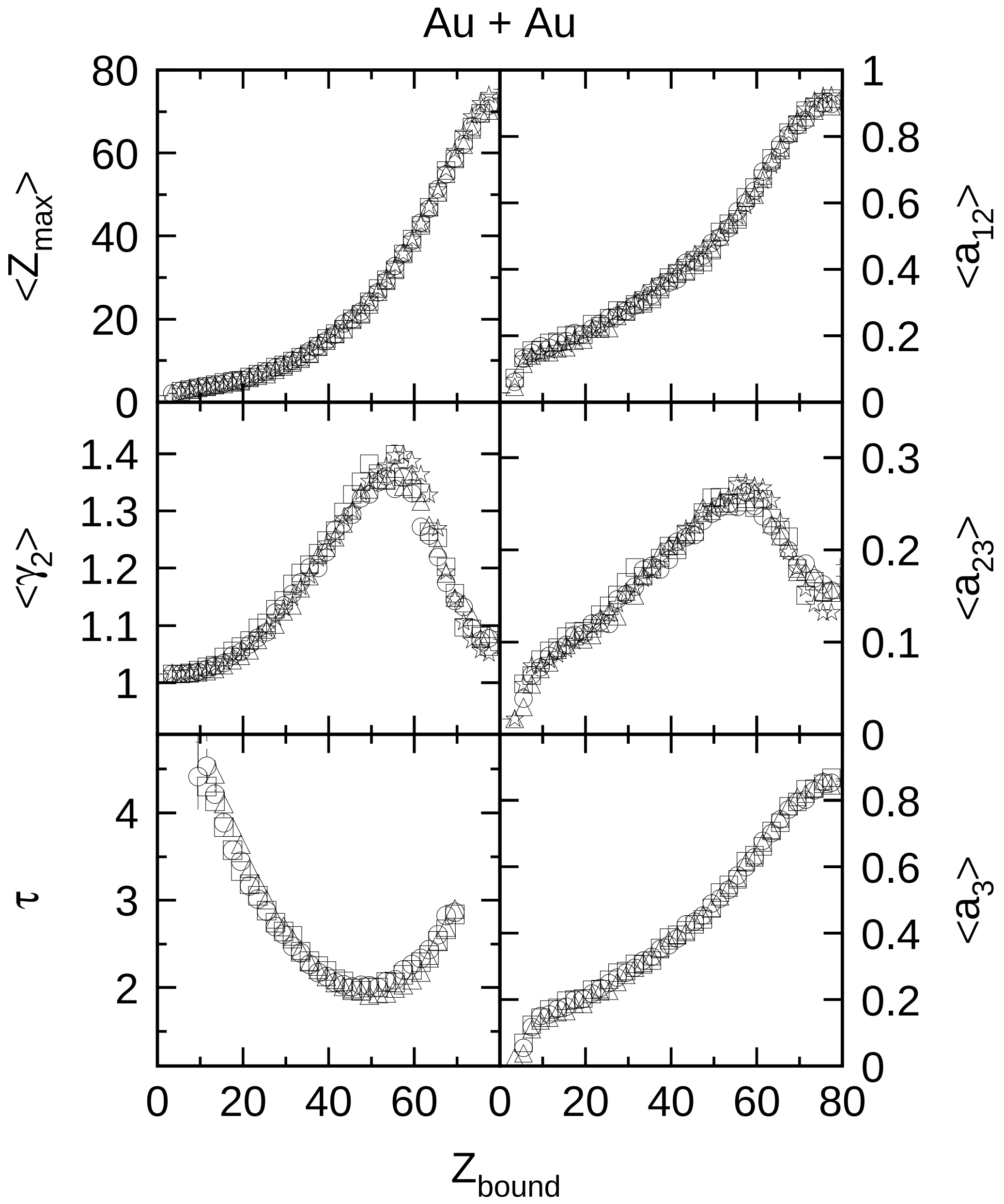

Figure 8: *Six charge-correlation observables as a function of* Z_{bound} *for the reaction* ^{197}Au *on* ^{197}Au*. The comparison is made for the four incident energies* $E/A = 400$*, 600, 800, and 1000 MeV in the top four panels and for three incident energies* E/A *= 600, 800, and 1000 MeV in the two bottom panels. The definitions are given in the text, the symbols have the same meaning as in fig. 6.*

largest fragment, and the three-fragment charge asymmetry

$$a_3 = \frac{\sqrt{(Z_{max} - \langle Z \rangle)^2 + (Z_2 - \langle Z \rangle)^2 + (Z_3 - \langle Z \rangle)^2}}{\sqrt{6} \cdot \langle Z \rangle} \tag{2}$$

where

$$\langle Z \rangle = \frac{1}{3} \cdot (Z_{max} + Z_2 + Z_3) \tag{3}$$

denotes the mean value of the three largest atomic numbers. The quantity a_3 assumes values near one when the partition is dominated by one heavy residue (large Z_{max}) and a value of zero when the three fragments are of equal size. Events containing at least two fragments with $Z \geq 2$ were selected for $\langle a_{12} \rangle$, and events containing at least three fragments with $Z \geq 2$ were selected for $\langle a_{23} \rangle$ and $\langle a_3 \rangle$.

The mean value of the normalized width of the fragment-charge distribution

$$\gamma_2 = 1 + \sigma^2(Z)/\langle Z \rangle^2 \tag{4}$$

peaks at $Z_{bound} = 55$ which is slightly larger than reported previously [3] for the reasons given above (fig. 8, middle, left). The Z spectra measured for given bins of Z_{bound} were fitted with power-law functions $\sigma(Z) \propto Z^{-\tau}$ over the range of intermediate-mass fragments. The resulting τ values (fig. 8, bottom, left) reach a minimum of $\tau = 2.0$ in the Z_{bound} range of 45 to 50. The characteristic dependence on the centrality of the collision is in good agreement with the results reported earlier [1, 3].

Once more, we emphasize the striking invariance of the partition patterns with the incident energy as evident from figs. 6 and 8. Although not specifically demonstrated in fig. 7, it is also valid for the mean multiplicities of the individual elements.

3.3 Accuracy of mean fragment multiplicity

The attainment of a maximum of relative accuracy in the measurements at different bombarding energies was one of the motivations for adopting a common definition of the spectator source. The absolute accuracy of the measured fragment multiplicities and charge correlations is influenced by several experimental effects. They will be listed and discussed in the following where we will focus on the maximum value of the $\langle M_{IMF} \rangle$ versus Z_{bound} correlation.

The upstream beam detectors, made of plastic scintillator foils with a resultant thickness of together 160 μm, represented a target of about $2{\cdot}10^{-3}$ interaction probability (not taking into account the hydrogen content). Coincident interactions of a beam particle in the scintillator foils and in the target are negligible. However, interactions in the scintillators may potentially lead to a valid trigger, although the trigger probability is relatively small due to the reduced solid angle subtended by the hodoscope with respect to the beam detectors. The recorded fragment multiplicities of these events, as a function of the recorded Z_{bound}, is slightly lower than that of reactions in the target, again due to the reduced solid angle. From analyzing data sets taken without a target, we find that the contamination caused by fragmentation reactions in the scintillator foils is indeed negligible. For the Au and U targets, since their interaction probabilities are the lowest, the relative contamination is the largest. Even in these cases, the contamination causes a reduction of the maximum mean multiplicity of only about 0.05 to 0.2 units, somewhat depending on the bombarding energy.

Secondary interactions within the target may change the fragment multiplicity on the percent level. The probability is largest for the lighter targets because of their larger interaction probability (up to 3.9%) but more violent interactions may occur in the heavier targets. The geometric acceptance of the Si-CsI(Tl) hodoscope relative to the subtended solid angle was 85%. The corresponding loss of light fragments, at the lower bombarding energies, can reach 0.1 units at the maximum. With the given detector geometry and adopted limit in rapidity (section 3.1) there was no dead area between the acceptances of the hodoscope and of the ALADIN magnet with the TOF wall.

Interactions with the pressure window (80-mg/cm^2 areal density, corresponding to about 1% interaction probability for heavy and less for lighter fragments) and with the counting gas behind the magnet may lead to additional secondary fragmentations of produced fragments, thereby causing both gains and losses in the number of intermediate-mass fragments. Finally, the remaining inefficiencies of the algorithms used for the TOF-wall analysis may lead to a misidentifications of fragments if secondary interactions within the wall are not recognized or double hits are not resolved. These effects may produce errors of different sign.

The estimate of the overall systematic uncertainty of the maximum mean fragment multiplicity yielded $\Delta\langle M_{IMF}\rangle = \pm\ 0.2$ (standard deviation). At the lower bombarding energies, caused by the fragment detection with the Si-CsI(Tl) hodoscope, the upper limit of the uncertainty increases up to $\Delta\langle M_{IMF}\rangle = +0.4$.

3.4 Dependence on projectile and target mass

The $\langle M_{IMF}\rangle$ versus Z_{bound} correlation depends on the mass of the projectile. The results obtained with the three projectiles ^{129}Xe, ^{197}Au, and ^{238}U at 600 MeV per nucleon show that, on the absolute scale, more fragments are produced in the decay of heavier projectiles (Fig. 9, left-hand side). However, a normalization with respect to the atomic number Z_P of the projectile reduces the three curves to a single universal relation (Fig. 9, right-hand side). Only TOF-wall data were used for this comparison as the pulse heights from the hodoscope were not recorded during the runs with the xenon beam. In addition, the upper limit of the Z range adopted for intermediate-mass fragments was changed from $Z \leq 30$ to $Z \leq Z_P/3$. This is meant to exclude fragments from binary-fission events. Since the elemental yields decrease rapidly with Z the exact location of this upper limit does not crucially affect this comparison of fragment multiplicities.

The target invariance of the M_{IMF} versus Z_{bound} correlation was first observed for collisions of ^{197}Au projectiles with C, Al, Cu, and Pb targets at 600 MeV per nucleon [1-4]. In fig. 10 (top) the universal nature of this correlation is demonstrated for ^{238}U projectiles at 1000 MeV per nucleon and for the full set of seven targets. With ^{238}U the maximum mean number of fragments ($3 \leq Z \leq 30$) is about five at $Z_{bound} = 50$. The spread over one half unit may not be significant in view of the systematic errors discussed in the last section. However, a slight tendency towards smaller multiplicities for the heavier targets can be explained by the larger Coulomb deflection that is caused by these targets and its effect on the acceptance for the very light fragments [26].

The reaction cross sections $d\sigma/dZ_{bound}$ are strongly target dependent [2, 10]. For ^{238}U projectiles of 1000 MeV per nucleon this is shown in the lower part of fig. 10. Only part of the Z_{bound} range can be covered with the lighter targets. The variation of $d\sigma/dZ_{bound}$

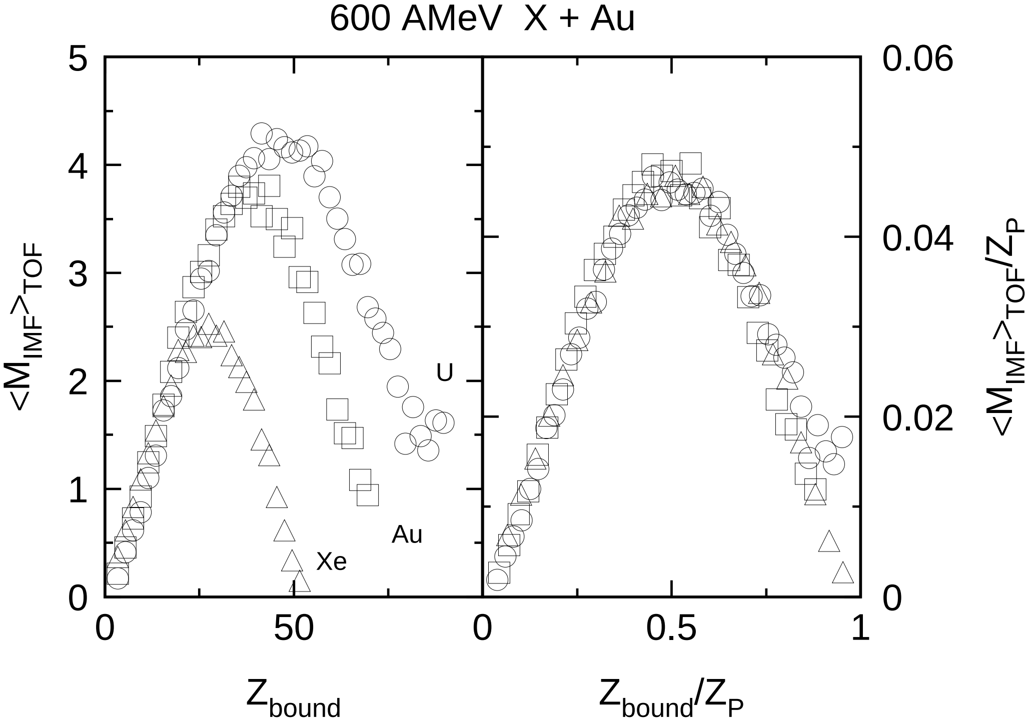

Figure 9: *Left panel: Mean multiplicity of intermediate-mass fragments* $\langle M_{IMF} \rangle_{TOF}$, *observed with the TOF wall, as a function of* Z_{bound} *for the reactions* ^{238}U *on* ^{197}Au *(circles),* ^{197}Au *on* ^{197}Au *(squares), and* ^{129}Xe *on* ^{197}Au *(triangles) at* $E/A = 600$ *MeV. Note that also in* Z_{bound} *only fragments detected with the TOF wall are included. Right panel: The same data, as shown in the left panel, after normalizing both quantities with respect to the atomic number* Z_P *of the projectile.*

with bombarding energy is insignificant for the collisions with heavy targets. There, the limit above which the spectator excitation is dominated by the collision geometry seems to be already reached. With the lighter targets, the higher bombarding energies allow for considerably larger energy transfers in central collisions. For ^{197}Au on Be, this is demonstrated in fig. 11. Collisions resulting in $Z_{bound} \approx 40$ and maximum fragment multiplicity (cf. fig. 6) are initiated with significant probability only at 1000 MeV per nucleon.

The same characteristic behavior is illustrated in an alternative way in fig. 12. Here the mean fragment multiplicities are given as a function of the impact parameter b for ^{197}Au projectiles and four targets at three bombarding energies. The impact parameter b was

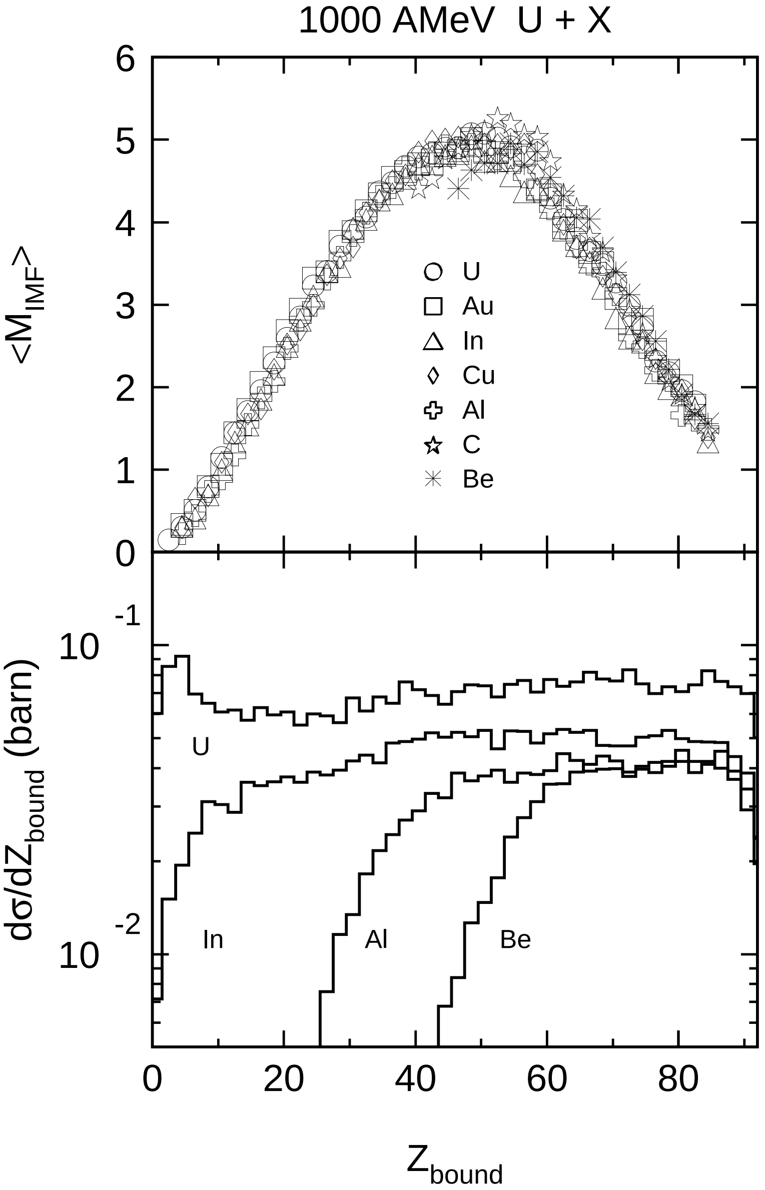

Figure 10: *Top: Mean multiplicity of intermediate-mass fragments* $\langle M_{IMF} \rangle$ *as a function of* Z_{bound} *for the reactions of* ^{238}U *projectiles at* $E/A = 1000$ *MeV with the seven targets of Be, C, Al, Cu, In, Au, and U. Bottom: Measured cross sections* $d\sigma/dZ_{bound}$ *for the reactions of* ^{238}U *projectiles at* $E/A = 1000$ *MeV with the four targets of Be, Al, In, and U. Note that the experimental trigger, for the case of uranium beams, affected the cross sections for* $Z_{bound} \geq 70$.

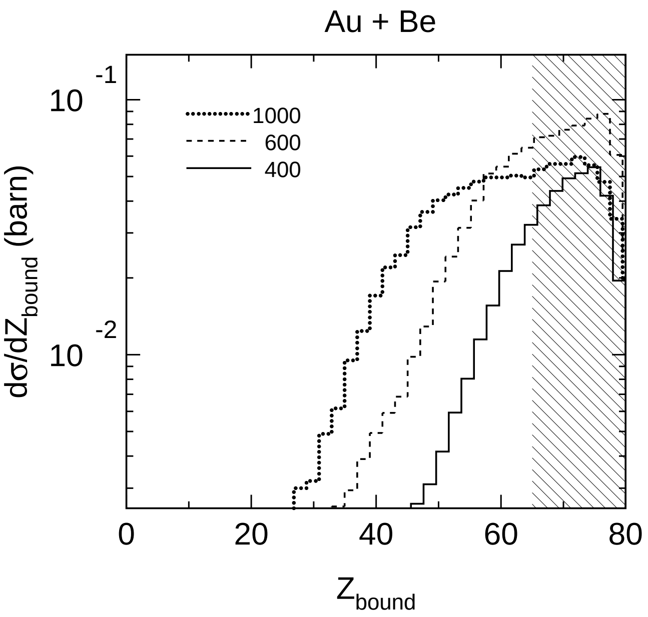

Figure 11: *Measured cross sections* $d\sigma/dZ_{bound}$ *for the reaction* ^{197}Au *on Be at* E/A *= 400 (full line), 600 (dashed), and 1000 MeV (dotted). Note that the experimental trigger conditions, which were not identical at the three bombarding energies, start to affect the cross sections at* Z_{bound} *between 60 and 70 (shaded area).*

derived by assuming that b is monotonically correlated with Z_{bound} (see ref. [2] for further details). With decreasing target mass the maximum fragment multiplicity is reached in more central collisions and the dependence on the bombarding energy increases. The data for the beryllium target, in particular, show that, at energies below 1000 MeV per nucleon, the spectators formed even in the most central collisions are not sufficiently excited to undergo a complete disassembly. The apparent decrease of $\langle M_{IMF} \rangle$ towards $b = 0$ for the very light Be and C targets is more likely to be caused by autocorrelations than by the mean behavior at small impact parameter. The bins of smallest impact parameter correspond to very small cross sections and are filled with the tails of events with the smallest values of Z_{bound} for which M_{IMF} is restricted by definition. This was verified by sorting the data measured at 400 MeV per nucleon according to the light particle multiplicity determined

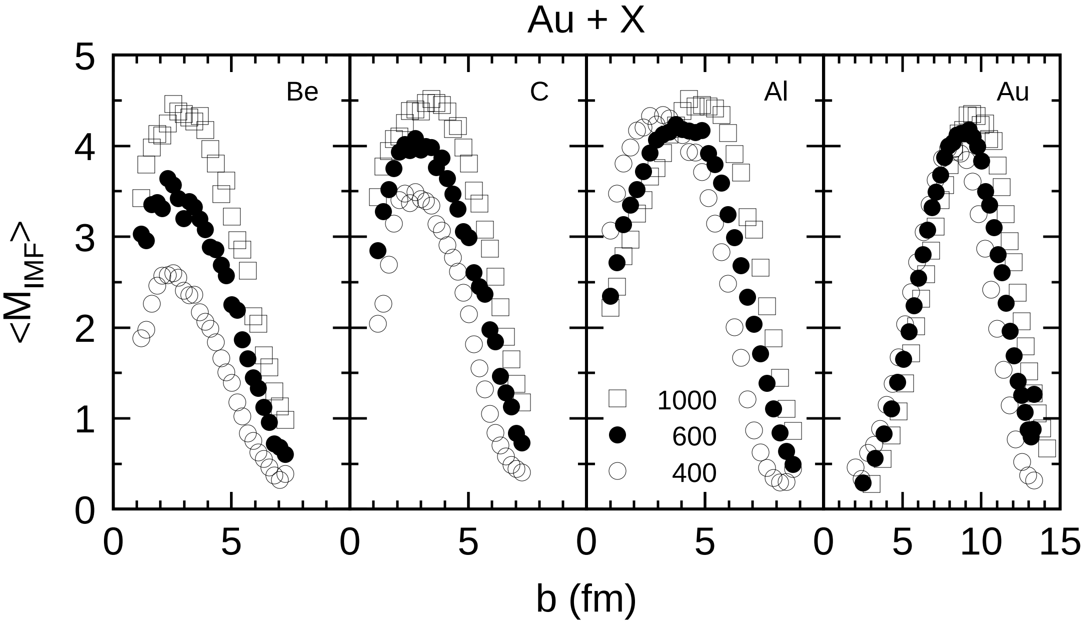

Figure 12: *Mean multiplicity of intermediate-mass fragments* $\langle M_{IMF} \rangle$ *as a function of the impact parameter b, as deduced from* Z_{bound}*, for the reactions* ^{197}Au *on Be, C, Al, and Au at three energies* E/A *= 400 (circles), 600 (dots), and 1000 MeV (squares).*

with the Miniball/wall and Si-CsI(Tl) hodoscope. In the latter case no comparable decrease is observed at the largest particle multiplicities.

3.5 Decay dynamics

The observed invariance of the transverse-momentum widths with respect to the bombarding energy (fig. 5) indicates that the entrance-channel dynamics play a minor role for the decay of the excited spectator. An estimate of the mean kinetic energies of the produced fragments in the moving frame was obtained in the following way: Event-by-event the vertical positions r_{yi} of all fragments measured with the TOF wall were converted into transverse momenta p_{yi} according to

$$p_{yi} = (r_{yi}/L_i) \cdot A_i \cdot p_P/A_P \tag{5}$$

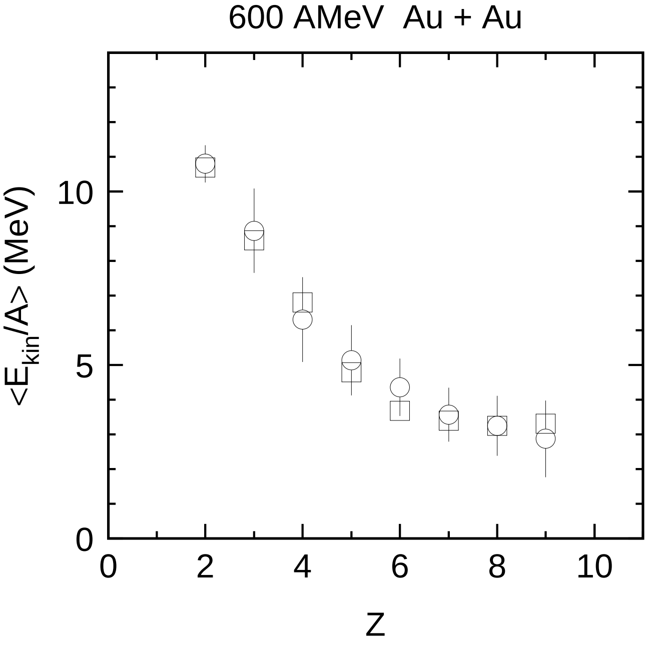

Figure 13: *Mean kinetic energies per nucleon in the moving frame, deduced from the transverse (circles) and longitudinal (squares) momentum widths as described in the text, for fragments from the reaction* ^{197}Au *on* ^{197}Au *at* E/A = *600 MeV and for 20* $\leq Z_{bound} \leq$ *60.*

Here the notation is the same as in eq. 1 with the additional subscript i denoting the fragment number within an event. With this information the center-of-mass motion of the decaying spectator in y direction and the intrinsic velocities of the fragments in this frame, in the y direction, were calculated. It was then assumed that the corresponding kinetic energies for one transverse degree of freedom represent one third of the total kinetic energies in the moving frame. Results for the reaction ^{197}Au on ^{197}Au at 600 MeV per nucleon, integrated over $20 \leq Z_{bound} \leq 60$, are given in fig. 13 (open circles). Because of the absence of a noticeable dependence on the bombarding energy (cf. fig. 5) they are representative for the whole energy range over which the universal spectator decay prevails. The assumption of dynamical equilibration over the three degrees of freedom was verified by using the measured velocities for the corresponding analysis in the longitudinal direction. The result, given by the open squares in fig. 13, turned out to be identical, within the errors.

The mean kinetic energies per unit fragment mass $\langle E_{kin}/A \rangle$ decrease rapidly with atomic number Z. In the limit of purely thermal contributions to the kinetic energies, $\langle E_{kin}/A \rangle$ is expected to have a $1/A$ dependence which is approximately observed. However, on the order of one half of the kinetic energies in the rest frame of the decaying system may originate from Coulomb repulsion and sequential decays of excited fragments [26]. With this assumption the magnitude of the kinetic temperature $T = 2/3 \cdot 1/2 \cdot \langle E_{kin} \rangle$ assumes a value of approximately 15 MeV. This exceeds considerably the emission temperatures $T \approx 5$ MeV derived from the relative isotopic abundances [17] or from relative yields of particle unbound states [27] which represents a well known but up to now not fully resolved problem [28-31]. Quantitatively, these values of the kinetic and the emission temperatures are in good agreement with those calculated by Bauer [31] who assumes that the higher kinetic temperatures reflect the additional Fermi momenta of the constituent nucleons of a fragment [32]. Small collective contributions to the kinetic energies can also have large effects on the apparent temperatures [33, 34]. On the other hand, the comparison with central collisions of ^{197}Au on ^{197}Au at 100 MeV per nucleon, made in ref. [35], shows that, in the present case of spectator decay, the upper limit for possible dynamical contributions is rather small. The kinetic energies are thus predominantly indicative of a thermally driven breakup out of an expanded state.

4 Discussion

4.1 Fragmentation at high bombarding energies

Exclusive fragmentation studies at high bombarding energies were performed by several groups [36-43]. The experiments using light projectiles of mass $A \leq 4$ confirm the finding that very high bombarding energies are needed in asymmetric systems in order to achieve the complete disassembly of a heavy spectator nucleus with large probability [37, 38]. These data fit rather well into the observed variation of the maximum mean multiplicity in central collisions with light targets (section 3.4).

A schematic representation of this systematic behavior, for reactions of gold nuclei with partners of different mass, is given in fig. 14. It includes the results obtained for ^{197}Au on ^{197}Au at lower energies [23] and for ^{84}Kr on ^{197}Au [44]. The figure shows the relation between the bombarding energy that is needed in order to observe maximum fragment production in central collisions and the mass number of the collision partner. For the reactions studied in this work in reverse kinematics, these energies may be taken from fig. 12: for ^{197}Au on C, e.g., the maximum fragment multiplicity is not reached with 600 but is easily reached with 1000 MeV per nucleon incident energy. In fact, already at 800 MeV per nucleon a considerable cross section is associated with a mean fragment multiplicity of ≈ 4.5 (data not shown in fig. 12).

The threshold energies of the other reactions were determined in a similar way. In the case of the ^{4}He on ^{197}Au reactions, a moderately complete excitation function is not available and the given value of 3.6 GeV per nucleon may represent an upper limit. At this energy the maximum of fragment production is reached, as has been argued on the basis of both the fragment multiplicity and the observation of a minimum in the τ parameter describing the elemental yields [37]. Light-particle induced reactions at significantly lower energies are incapable of producing spectators at sufficiently high excitation. This is evident from the excitation energies of $E_x/A \leq 3$ MeV for collisions of ^{1}H and ^{3}He projectiles of 2-GeV total energy with gold targets, deduced from neutron multiplicity measurements [45], and consistent with the relatively small mean fragment multiplicities reported for ^{3}He on ^{197}Au at 1.6 GeV per nucleon [38] and ^{4}He on ^{197}Au at 1.0 GeV per nucleon [37]. For this latter group of reactions, the fragment multiplicity is still on the rising side where the partitions are characterized by one large fragment (large Z_{max}) and a correspondingly large first asymmetry a_{12} (cf. fig. 8). This is the regime of residue formation (fig. 14). On the other hand, with collision partners of masses or energies exceeding the optimum values, the central collisions will lead to spectators of decreasing mass and to their disassembly into an increasingly larger number of light fragments and particles and, eventually, to vaporization [23, 24].

High charge resolution and full phase space coverage above the identification threshold of $Z \geq 6$ has been achieved with plastic nuclear track detectors [39, 46]. For a comparison

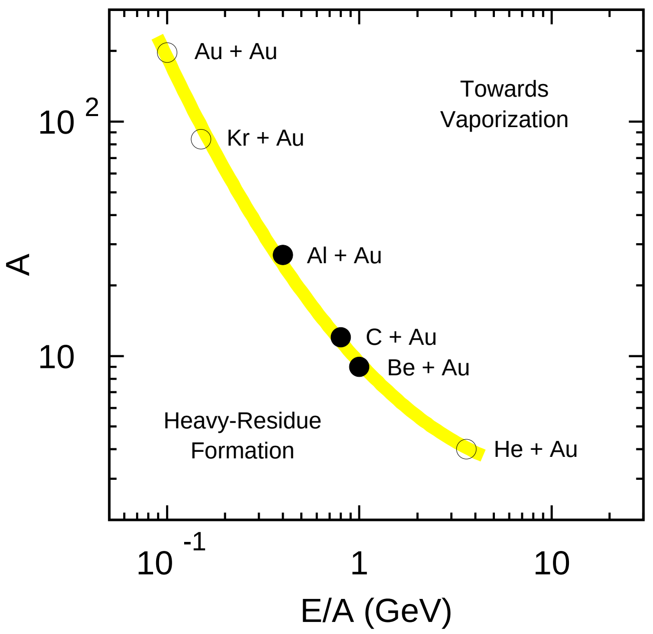

Figure 14: *Mass number A of the collision partner versus bombarding energy for reactions of* ^{197}*Au nuclei for which maximum fragment production has been observed in central collisions. Full points denote reactions studied in this work in reverse kinematics, open symbols refer to work reported in [23, 37, 44].*

with the results of the Siegen group [39], obtained at the Bevalac with ^{197}Au beams in the range of 0.85 to 1 GeV per nucleon, a threshold of $Z \geq 6$ was applied to our data. The sorting variable Z_{bound} was replaced by Z_{b6} which represents the sum of the atomic numbers Z_i of all fragments with $Z_i \geq 6$. The correlation between the mean multiplicities $\langle M_{IMF6} \rangle$ of fragments with $6 \leq Z \leq 30$ and Z_{b6} is shown in fig. 15. A maximum of $\langle M_{IMF6} \rangle \approx 2$ is reached for Z_{b6} between 20 and 30. The data measured with carbon targets in the two experiments agree quantitatively with each other within the quoted errors (cf. fig. 7 of ref. [39]). This mutually confirms the experimental and analysis techniques. The small reduction of $\langle M_{IMF6} \rangle$ with increasing mass of the target, reported by the Siegen group, is less pronounced in our data (figs. 10 and 15). The mean multiplicities $\langle M_{IMF6} \rangle$ in the range $20 \leq Z_{b6} \leq 30$ differ by 4% ± 2% for the C and Au targets. In fact, we find that the

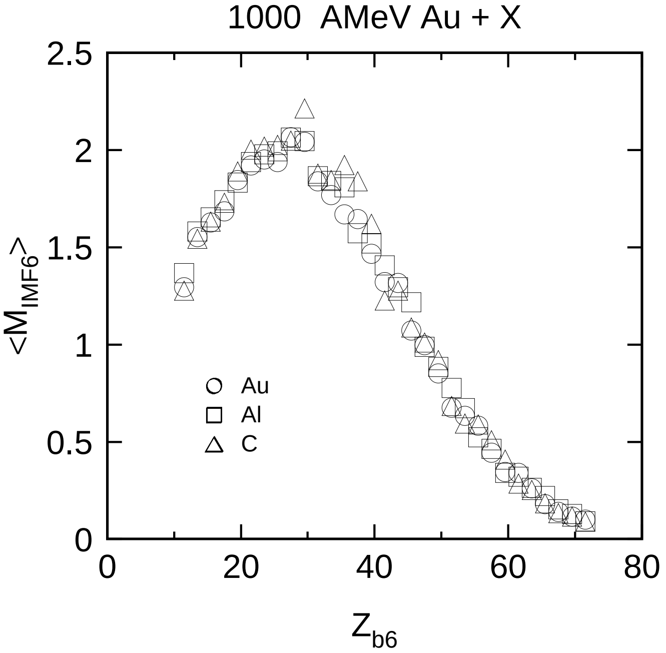

Figure 15: *Mean multiplicity* $\langle M_{IMF6} \rangle$ *of intermediate-mass fragments with* $Z \geq 6$ *as a function of the bound charge* Z_{b6} *(see text) for the reactions* ^{197}*Au on C, Al, and Au at* $E/A = 1000$ *MeV.*

invariance with respect to the target and with respect to the bombarding energy holds for arbitrary choices of a lower threshold in Z. This is true also for the correlation observables displayed in fig. 8.

Emulsion targets were used by Jain and Singh in their study of the fragmentation of ^{84}Kr beams of 1.52 GeV per nucleon, performed at the Bevalac [40]. They observe a maximum multiplicity of $\langle M_{IMF} \rangle$ of 1.8 to 2.0. This corresponds to $\langle M_{IMF} \rangle / Z_P = 0.053$ which is in excellent agreement with the present results for Au and U beams (figs. 6 and 10), thus extending the invariance with respect to the bombarding energy and the projectile mass over a wider range. Note that the slightly lower multiplicities shown in fig. 9, measured with the TOF wall at 600 MeV per nucleon incident energy, do not include the fragments detected with the hodoscope.

In their work, performed at the AGS in Brookhaven, Jain *et al.* have studied the fragmentation of ^{197}Au projectiles at 10.6 GeV per nucleon [41]. The fragment charges were deduced from δ-ray counts. The fragment multiplicities, charge asymmetries, and widths of the charge distributions at this high energy are very similar to those measured at 1 GeV per nucleon and below. Jain *et al.* show a comparison with the results reported by Hubele *et al.* [2], measured at 600 MeV per nucleon and with the acceptance given by the TOF wall of 1-m length. With the acceptance offered by the extended TOF wall and with the source definition adopted in the present work, the maximum of the $\langle M_{IMF} \rangle$ versus Z_{bound} correlation is at $Z_{bound} = 40$ which coincides with the result found at 10.6 GeV per nucleon. However, the maximum number of intermediate-mass fragments of 3.5, as reported by Jain *et al.*, is about one unit below the values obtained in the present work.

The fragmentation of ^{197}Au projectiles of 10.6 GeV per nucleon in collisions with emulsion targets was also investigated by the KLMM Collaboration [42, 43]. In their more recent report [43] these authors present a rather detailed comparison with the data of Hubele *et al.* [2] and Kreutz *et al.* [3]. Some of the conclusions are modified if the comparison is made with the new data of this work. We find that the correlations of Z_{max} with Z_{bound}, measured at 10.6 GeV per nucleon and at ≤ 1 GeV per nucleon, agree now perfectly. Good agreement is also observed for the charge variance $\langle \gamma_2 \rangle$ (eq. 4). However, the maximum value of $\langle M_{IMF} \rangle$ of 3.2, reached at $Z_{bound} \approx 45$ and in good agreement with the data of ref. [41], is one unit lower than measured in this work. By comparing the multiplicities as a function of Z we have identified the difference as mainly occuring in the yields of very light fragments. A maximum mean multiplicity for $3 \leq Z \leq 6$ of 1.8 is reported for 10.6 GeV per nucleon while it is 3.0 in our data in the same Z range (cf. fig. 7). The difference in the maximum mean He multiplicity (6.5 at the higher and 4.5 at the lower bombarding energies) may be partly due to the rapidity limit applied in the present work (fig. 4). It is not excluded, at present, that the differences may reflect a weak variation of the fragmentation pattern with bombarding energy; on the other hand, emulsion data measured at 1 GeV per nucleon [36] were shown to agree with those for 10.6 GeV per nucleon over a major part of the Z_{bound} range [43].

The KLMM collaboration has reported Z_{bound} distributions which are sorted individually for reactions on the light (H, C, N, and O) and on the heavy constituents of the emulsion target [42]. Qualitatively, the distribution for the light constituents decreases with decreasing Z_{bound} in a similar way as the distributions for light targets in the present work. On the more quantitative level, however, the closest resemblance is with the distribution measured for the ^{197}Au on Al reaction at 1000 MeV per nucleon rather than the ^{197}Au on C reaction at this energy. This might be considered as another indication of the role of the bombarding energy in reaching large cross sections for high-multiplicity breakups in asymmetric systems.

Towards higher bombarding energies, no limit for the universality of the spectator fragmentation is known at present. Limiting fragmentation, i.e. a saturation of the production cross sections for intermediate-mass fragments at bombarding energies in excess of several GeV, has been observed [47-49]. It is also an experimentally established fact that the elemental distributions change very little at high bombarding energies [50, 51]. This suggests that the cross sections for the formation of highly excited spectator nuclei may be rather weak functions of the bombarding energy in the GeV range. In a pure abrasion picture this is expected since the cross section and the excitation energy are mutually interrelated via their geometric dependence on the impact parameter [52]. On the other hand, it is known that the geometric abrasion model can only account for part of the excitation energy deposited in the formed spectator nuclei [53]. The missing part is thought to be due to struck nucleons and secondary particles being scattered into the cold spectator matter. Some of these particles may be deltas and other nucleon resonances which carry additional energy. It is known from experiment that the cross sections and transverse momentum distributions of scattered or produced particles change very slowly at high bombarding energies [54, 55]. Thus, also these factors will not introduce a dramatic energy dependence. One may therefore conclude that the spectator formation and decay, as observed in the present work, persists up to the highest bombarding energies with virtually invariant features.

4.2 Model calculations

Model calculations were performed in order to identify possible reasons for the observed Z_{bound} universality. The excitation of the primary spectator nucleus as a function of the number of abraded nucleons was studied with the intranuclear-cascade model. A recent version of the ISABEL code by Yariv and Fraenkel with the slow rearrangement option was used [25, 56]. Less emphasis was given to the absolute values of the excitation energies, which may be overestimated by this model (see next section), than to their systematic behavior.

The obtained results, calculated for collisions of ^{197}Au projectiles with different targets, reflect the universality seen in the experiment. The slopes of the correlation of the mean specific excitation energy $\langle E_x/A \rangle$ with the mass A_0 of the primary projectile spectator are found to be independent of the bombarding energy and of the mass of the target (fig. 16, note the offsets in A_0). Primary spectators of a given mass seem to always have the same invariant excitation energy. Therefore, if the subsequent decay proceeds statistically, the same universal fragmentation patterns will be observed in the corresponding regions of Z_{bound}. It is further found that the maximum of the specific excitation energy that can be reached with a given target depends strongly on the target mass and, less dramatically, on the bombarding energy (figs. 16 and 17). Also these features are consistent with the experimental observations (section 3.4).

The fairly weak variation with the bombarding energy may seem somewhat surprising since the excitation of Δ resonances has been suggested to be an efficient means of energy dissipation [57-59]. The rate of Δ production grows rapidly with bombarding energy in the range 400 to 1000 MeV per nucleon, as evident from measured pion yields [60, 61]. Consequently, the cross sections for the production of spectators with high excitation energy may be expected to increase as well. This is only partly confirmed by the calculations. If the code is modified, so as to suppress the production of Δ resonances, the specific excitation energies as a function of the impact parameter are only slightly lower, even at the higher bombarding energies (fig. 17). There, however, and, in particular for the lightest targets, the heating by Δ excitation may be important on a quantitative level and may determine whether the maximum of fragment production can be observed in a given collision system (cf. previous section). We notice that, in contrast to $\langle E_x/A \rangle$ versus b, the relation $\langle E_x/A \rangle$ versus A_0 does not depend on whether Δ production is included or suppressed in the calculations (fig. 16, right-most panel). It does not respond to this modification of the

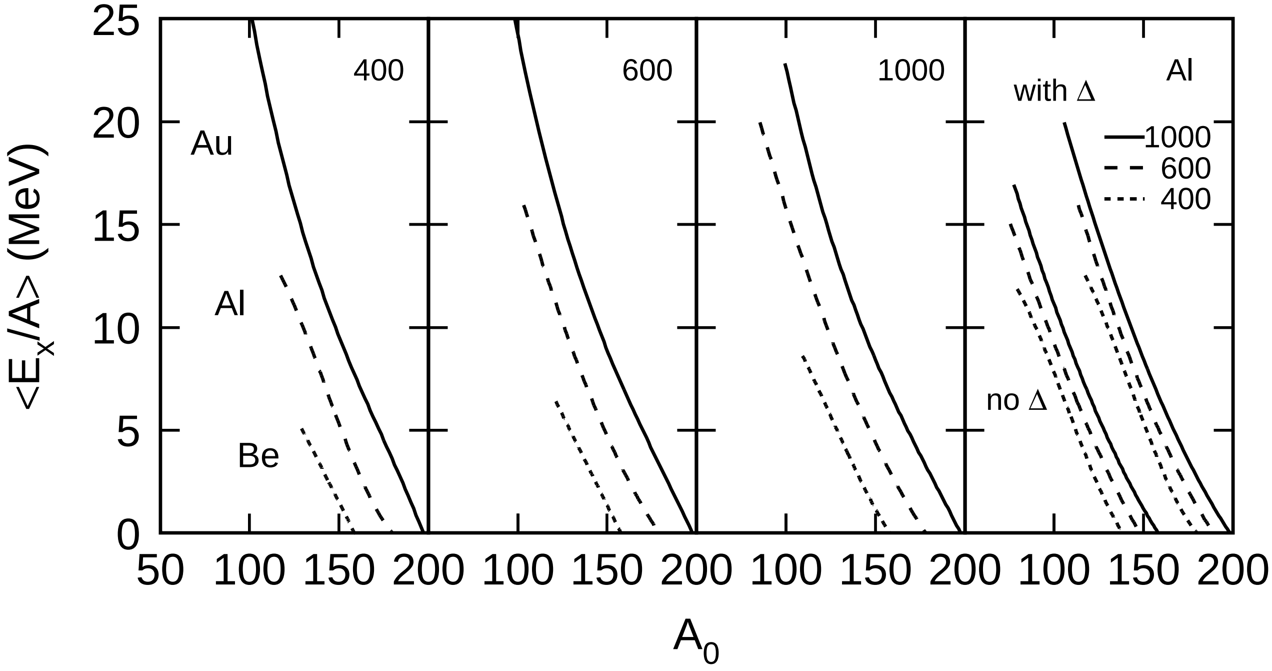

Figure 16: *Results of the intranuclear-cascade calculations: Mean specific excitation energy* $\langle E_x/A \rangle$ *as a function of the mass number* A_0 *of the primary spectator for the reactions* ^{197}Au *on Be, Al, and Au targets at three bombarding energies* E/A = *400 MeV (left-most panel), 600 MeV (middle-left), and 1000 MeV (middle-right). The right-most panel shows the results with and without* Δ *production for the case of the Al target and for the three incident energies. All curves start at* A_0 = *197 and have nearly the same slopes. For the purpose of illustration the following offsets were applied: in the first three panels 20 units of* A_0 *for each consecutive target and, in the last panel, 10 units of* A_0 *between consecutive lines within a group and 40 units between the two groups.*

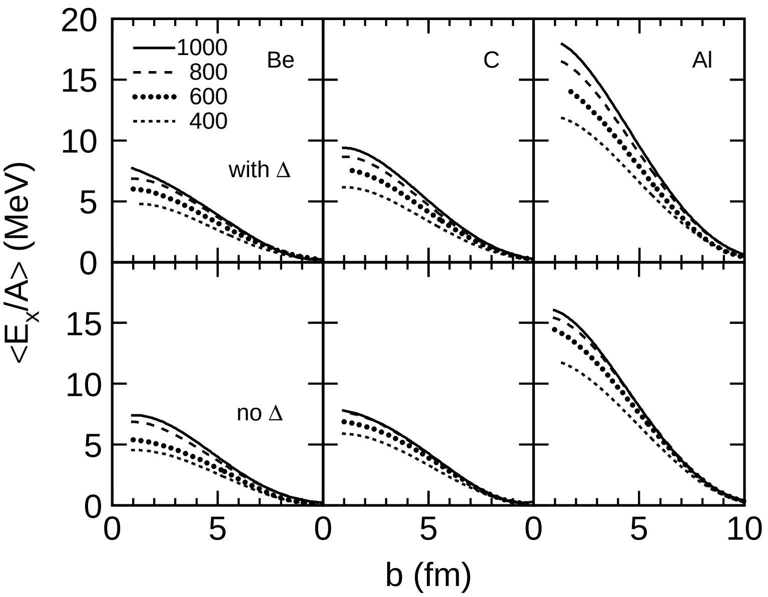

Figure 17: *Results of the intranuclear-cascade calculations: Mean specific excitation energy* $\langle E_x/A \rangle$ *of the primary spectator as a function of the impact parameter* b *for the reactions* ^{197}Au *on Be, C, and Al targets at four bombarding energies* $E/A =$ *400, 600, 800, and 1000 MeV. The upper (lower) row of panels shows the results with (without)* Δ *production.*

heating mechanism. As outlined above, it is essentially the invariance of this function which is responsible for the observed Z_{bound} universality. For the case of hadron induced reactions, this invariant feature has been known since the early intranuclear-cascade models were developed [62].

The results of the calculations also exhibit the linear scaling with the projectile mass seen in the experiment (section 3.4). The slopes of $\langle E_x/A \rangle$ versus A_0 grow steeper with decreasing mass of the projectile but are the same when plotted versus A_0/A_P (fig. 18). This behavior is expected for the purely geometric abrasion. The intranuclear-cascade calculations demonstrate that this feature is not altered by the additional mechanisms of spectator excitation.

It is not a priori obvious why the linear scaling with the projectile mass should be

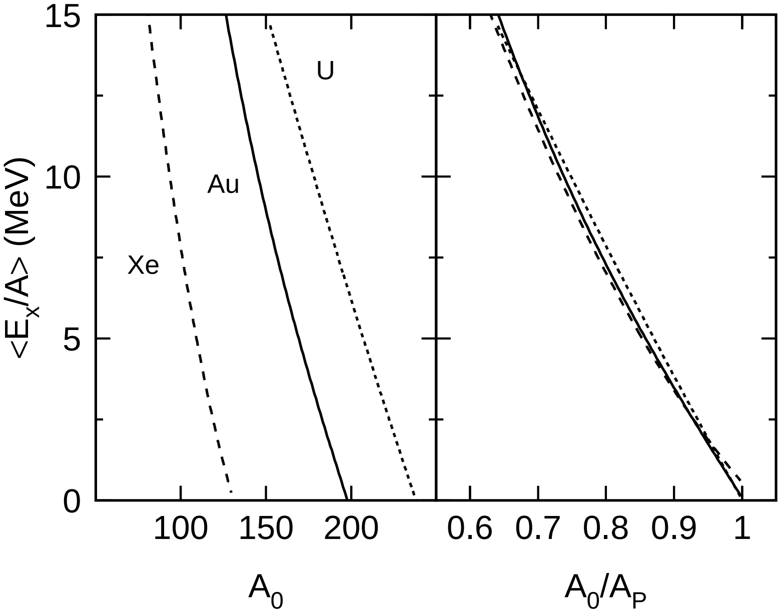

Figure 18: *Results of intranuclear-cascade calculations:*
Left panel: Mean specific excitation energy $\langle E_x/A\rangle$ *as a function of the mass* A_0 *of the primary spectator for the reactions of* ^{238}U, ^{197}Au, *and* ^{129}Xe *on a Au target at* E/A = *600 MeV. The calculations were restricted to impact parameters* $b \geq 8$ *fm.*
Right panel: The same correlations plotted as a function of the reduced mass number A_0/A_P.

preserved during the statistical decay. The surface energies play an important role in the multi-fragment decays, and the ratio of surface to volume of the decaying system may not be unimportant. Calculations within the statistical multifragmentation model show, however, that effects of this origin are not significant in the range of projectile masses from krypton to uranium (fig. 19). The Berlin model in the version implemented in the code McFRAG [63] was used. In these calculations the mass A_0 and charge Z_0 were kept fixed while E_x/A was varied. This ignores the correlation between excitation energy and mass of the primary spectator, caused by the primary reaction stage, and results in much larger peak multiplicities than experimentally observed. The figure, nevertheless, demonstrates that both scaled functions $\langle Z_{bound}\rangle/Z_0$ and $\langle M_{IMF}\rangle/Z_0$ follow universal curves as a function

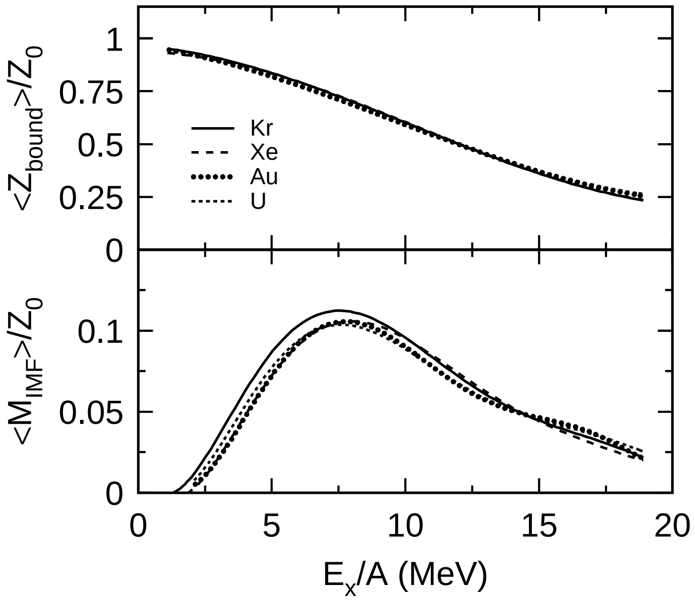

Figure 19: *Results of calculations with the statistical multifragmentation model, performed with the code McFRAG [63]: Reduced variables* $\langle Z_{bound}\rangle/Z_0$ *(top) and* $\langle M_{IMF}\rangle/Z_0$ *(bottom) as a function of the specific excitation energy* E_x/A *for the four cases of excited Kr, Xe, Au, and U nuclei.*

of the specific excitation energy E_x/A. Combined with the intranuclear-cascade relation between $\langle E_x/A\rangle$ and A_0/A_P (fig. 18), the model result is compatible with the observed dependence on the projectile mass. The top part of fig. 19, furthermore, illustrates how Z_{bound}, according to the model, increasingly deviates from the charge Z_0 of the produced spectator system as its excitation energy increases.

The link between the first and the later reaction stages is a subject of high current activity (see, e.g., [5, 64, 65]). This concerns the expansion and equilibration which are thought to have occurred prior to the fragment decay described by the statistical multifragmentation models. Intuitively, one may suspect that the random knockout of nucleons from and the injection of nucleons into the primary spectator produce a highly disordered system capable of rapidly evolving towards equilibrium. The origin of the Z_{bound} universality may thus be primarily seen in the stochastic nature of the initial cascade process.

4.3 Energy deposition

A quantitative knowledge of the energy transfer to the primary spectator is indispensable for any interpretation of the multi-fragment decay in terms of nuclear-matter properties. On the other hand, the transient nature of the excitation and decay processes makes it difficult to arrive at a consistent definition of the spectator system and its associated excitation energy. The present situation is summarized in fig. 20 which shows the results of six analyses for spectators from ^{197}Au collisions with either Au or Cu targets as a function of Z_{bound}. The types of analysis are qualitatively different, relying either on model calculations, on the experimental results or on both. To permit the comparison in a single figure, results calculated as a function of the impact parameter b were converted to the Z_{bound} scale by using the derived empirical relations between the two quantities (section 3.4).

The highest energy deposits in the spectator system are obtained with the intranuclear-cascade model (cf. previous section). They represent the sum of the hole energies left behind by nucleons knocked-out from the spectator and of the energies carried by struck nucleons captured into the spectator (the threshold parameter was set to 14 MeV). Since the evolution of the spectator is ignored these values may be considered as upper limits. Considerably lower excitation energies were obtained with the Boltzmann-Uehling-Uhlenbeck (BUU, [66]) model as reported in ref. [3]. There, the spectator was defined and analyzed after the system had evolved for a time of 60 to 100 fm/c under the influence of the mean field. At that time, as it was found for the calculations, most fireball-like nucleons have left the reaction zone.

The lowest estimates of the excitation energy result from the analyses of the earlier ^{197}Au on Cu data at 600 MeV per nucleon [3] performed with the statistical multifragmentation models [5-7,10,67]. There, in order to reproduce the observed multiplicities and charge correlations of intermediate-mass fragments, an ensemble of equilibrated residual nuclei was needed which is characterized by a saturation of the excitation energy at about

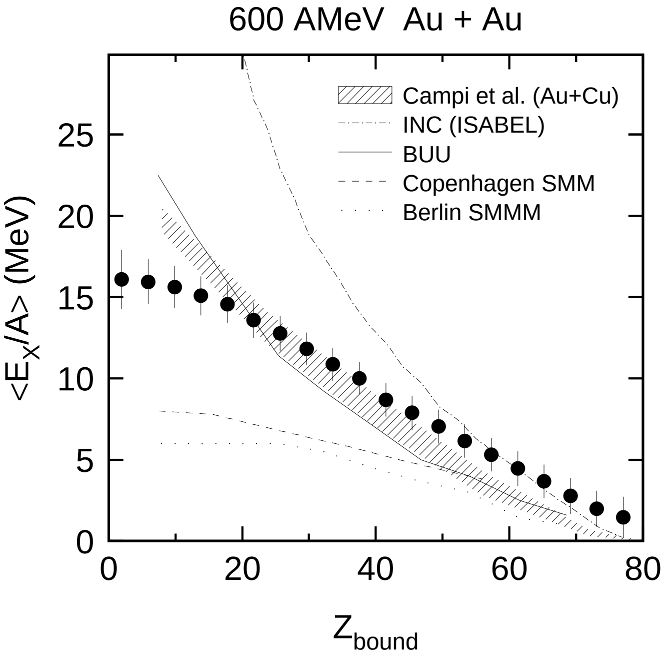

Figure 20: *Excitation energy per nucleon* E_x/A *as a function of* Z_{bound}. *The data points give the results deduced from summing up the breakup Q values, calculated for the observed partitions, and the kinetic energies for the reaction* ^{197}Au *on* ^{197}Au *at* $E/A = 600$ *MeV. The shaded area and the lines represent the results of the analysis by Campi et al. [70], of the intranuclear-cascade (this work) and the BUU calculations [3], and of the analyses with the Copenhagen [6] and Berlin [7] statistical multifragmentation models, all for the reaction* ^{197}Au *on Cu at* $E/A = 600$ *MeV. When necessary, the impact parameter b was converted into* Z_{bound} *by using the empirical relation obtained for the* ^{197}Au *on Cu reaction.*

8 MeV per nucleon if the Copenhagen or Moscow models are used [5, 6, 10, 67]. With the Berlin version of the statistical multifragmentation model a saturation energy as low as 6 MeV per nucleon was obtained [7]. The systematic study of the complex correlation between the observables and the code input parameters has shown, however, that the deduced saturation energy depends sensitively on the measured mean fragment multiplicity [67]. The present data, exhibiting slightly higher mean multiplicities, therefore lead to excitation energies that may reach up to about 12 MeV per nucleon at small Z_{bound} [68, 69].

A method to determine the excitation energy from the experimental data alone, without relying on a reaction model, was first presented by Campi *et al.* [70] and applied to the earlier ^{197}Au + Cu data. After having determined the yields of hydrogen isotopes by extrapolating to $Z = 1$ from the measured abundances for $Z \geq 2$, these authors estimated the energy residing in the breakup Q value and in the kinetic energies of the final fragments. The asymptotic value of $E_x/A = 23$ MeV at $Z_{bound} = 0$ is the sum of the binding energy of 8 MeV and the kinetic energy of 15 MeV assigned to nucleons. In the same type of analysis with the present data for ^{197}Au + ^{197}Au at 600 MeV per nucleon, the measured neutron multiplicities and their kinetic energies in the projectile frame were taken into account [17]. Solving the balance equations for energy, mass, and charge with this additional information yields a larger number of composite particles, correspondingly less free nucleons, and smaller excitation energies. A maximum of $E_x/A = 15$ MeV for $Z_{bound} \leq 10$ was reported in ref. [17]. The data points shown in fig. 20 are the result of a new analysis with the same method from which excitation energies up to a maximum of 17 MeV per nucleon are obtained. The development of this method is still in progress and further small changes are not excluded.

The BUU estimate seems to come closest to the two experimental determinations of the available decay energy which fall in between the differing estimates with the intranuclear cascade and the statistical multifragmentation models. Assuming that all analyses are realistic within their own frameworks, the observed ordering is quite reasonable in the sense that the formation of the equilibrated spectator in the primary reaction stages and its evolution towards the final breakup stage may be accompanied by the emission of fast light particles and thus by a loss of excitation energy. In addition, small collective contributions due to rotation or flow will also cause differences between the measured energies and those derived from statistical analyses of the exit channel configurations. The more recent results obtained with the statistical multifragmentation models narrow this gap but still leave room for a substantial preequilibrium stage or a small collective component, even though no positive evidence for either one has emerged from the present work. At $Z_{bound} \approx 40$, where the fragment multiplicity reaches its maximum, the experimentally determined excitation energies are between 8 and 10 MeV per nucleon, close to the mean binding energy of nuclei.

5 Conclusion

The systematic set of data, measured from 400 up to 1000 MeV per nucleon incident energy, reveals the universal nature of multi-fragment decays of excited spectator nuclei at relativistic energies. It suggests that the correlation of excitation energy and mass of the produced spectator systems and the statistical nature of their decay remain virtually unchanged over the studied range of bombarding energies. In reactions with the lighter targets, specific minimum values of the bombarding energy have to be exceeded in order to reach the maximum fragment multiplicities and to achieve a complete disassembly of the projectile spectator. The corresponding lower limits are about 400, 800, and 1000 MeV per nucleon for collisions of gold projectiles with aluminum, carbon, and beryllium targets, respectively.

The results of calculations with the intranuclear cascade and statistical multifragmentation models permit a qualitative understanding of the observed universality. The calculations as well as comparisons with emulsion data for collisions at higher incident energies suggest that the identified production and fragmentation of excited spectator nuclei may persist up to very high energies with virtually invariant properties and slowly changing cross sections. In the pure abrasion picture, this follows from the mutual connection between excitation energy and cross section via their geometric dependence on the impact parameter. The additional mechanism of spectator heating by scattered nucleons or produced particles is not expected to significantly modify this picture.

The observed decoupling from the entrance-channel dynamics strongly suggests that the multi-fragment decay of the spectator occurs after it has reached statistical equilibrium. The isotropy in the rest frame of the spectator and the Z dependence of the intrinsic fragment momenta indicate that this includes the kinetic degrees of freedom. Statistical interpretations were shown to be applicable, and the fragmentation seems to be mainly governed by the deposited excitation energy. The fragment multiplicities rise with excitation energy until a maximum is reached at about 8 to 10 MeV per nucleon, as experimentally determined for reactions with Au projectiles. For the more violent collisions in the regime of decreasing fragment multiplicities, the estimates of the energy deposited in the decaying spectator system disagree more widely, thus leaving room for a possibly important role of preequilibrium emission. This problem will need further attention if the study of equilibrium properties of nuclear matter is to be extended to these very high excitation energies.

The authors wish to thank the staff at SIS and GSI for the excellent working conditions and J. Lühning and W. Quick for the technical support provided. Useful discussions with A.S. Botvina and H.C. Britt are gratefully acknowledged. J.P. and M.B. acknowledge the financial support of the Deutsche Forschungsgemeinschaft under the Contract No. Po 256/2-1 and Be1634/1-1, respectively. W.G.L. and L.G.S. acknowledge the receipt of U.S. Presidential Young Investigators Awards. This work was supported by the European Community under contract ERBCHGE-CT92-0003 and ERBCIPD-CT94-0091, by the National Science Foundation under Grants No. PHY-90-15255 and No. PHY-92-14992, and by the U.S. Department of Energy under Contract No. DE-FG02-87ER-40316.

References

[a] Present Address: Chalk River Laboratories, Chalk River, Ontario K0J 1J0, Canada

[b] On leave from the Comision Nacional Energia Atomica, Argentina

[c] Present Address: Department of Chemistry, Indiana University, Bloomington, IN 47405, USA

[d] Present address: National Superconducting Cyclotron Laboratory, Michigan State University, East Lansing, MI 48824, USA

[e] Present address: Nuclear Science Division, Lawrence Berkeley Laboratory, Berkeley, CA 94720, USA

[f] Present address: Department of Physics, Massachusetts Institute of Technology, Cambridge, MA 02139, USA

[g] Present address: Physics Department, Hope College, Holland, MI 49223, USA

[h] Present address: Max-Planck-Institut für Kernphysik, D-69117 Heidelberg, Germany

[1] C.A. Ogilvie, J.C. Adloff, M. Begemann–Blaich, P. Bouissou, J. Hubele, G. Imme, I. Iori, P. Kreutz, G.J. Kunde, S. Leray, V. Lindenstruth, Z. Liu, U. Lynen, R.J. Meijer, U. Milkau, W.F.J. Müller, C. Ngô, J. Pochodzalla, G. Raciti, G. Rudolf, H. Sann, A. Schüttauf, W. Seidel, L. Stuttge, W. Trautmann, and A. Tucholski, Phys. Rev. Lett. 67 (1991) 1214

[2] J. Hubele, P. Kreutz, J.C. Adloff, M. Begemann–Blaich, P. Bouissou, G. Imme, I. Iori, G.J. Kunde, S. Leray, V. Lindenstruth, Z. Liu, U. Lynen, R.J. Meijer, U. Milkau, A. Moroni, W.F.J. Müller, C. Ngô, C.A. Ogilvie, J. Pochodzalla, G. Raciti, G. Rudolf, H. Sann, A. Schüttauf, W. Seidel, L. Stuttge, W. Trautmann, and A. Tucholski, Z. Phys. A 340 (1991) 263

[3] P. Kreutz, J.C. Adloff, M. Begemann–Blaich, P. Bouissou, J. Hubele, G. Imme, I. Iori, G.J. Kunde, S. Leray, V. Lindenstruth, Z. Liu, U. Lynen, R.J. Meijer, U. Milkau,

A. Moroni, W.F.J. Müller, C. Ngô, C.A. Ogilvie, J. Pochodzalla, G. Raciti, G. Rudolf, H. Sann, A. Schüttauf, W. Seidel, L. Stuttge, W. Trautmann, and A. Tucholski, Nucl. Phys. A556 (1993) 672

[4] J. Hubele, P. Kreutz, V. Lindenstruth, J.C. Adloff, M. Begemann–Blaich, P. Bouissou, G. Imme, I. Iori, G.J. Kunde, S. Leray, Z. Liu, U. Lynen, R.J. Meijer, U. Milkau, A. Moroni, W.F.J. Müller, C. Ngô, C.A. Ogilvie, J. Pochodzalla, G. Raciti, G. Rudolf, H. Sann, A. Schüttauf, W. Seidel, L. Stuttge, W. Trautmann, A. Tucholski, R. Heck, A.R. DeAngelis, D.H.E. Gross, H.R. Jaqaman, H.W. Barz, H. Schulz, W.A. Friedman, and R.J. Charity, Phys. Rev. C46 (1992) R1577

[5] A.S. Botvina and I.N. Mishustin, Phys. Lett. B294 (1992) 23

[6] H.W. Barz, W. Bauer, J.P. Bondorf, A.S. Botvina, R. Donangelo, H. Schulz, and K. Sneppen, Nucl. Phys. A561 (1993) 466

[7] Bao-An Li, A.R. DeAngelis, and D.H.E. Gross, Phys. Lett. B303 (1993) 225

[8] J. Konopka, G. Peilert, H. Stöcker, and W. Greiner, Prog. Part. Nucl. Phys. 30 (1993) 301

[9] Zheng Yu-Ming, Wang Fei, Sa Ben-Hao, and Zhang Xiao-Ze, Phys. Rev. C53 (1996) 1868

[10] A.S. Botvina, I.N. Mishustin, M. Begemann–Blaich, J. Hubele, G. Imme, I. Iori, P. Kreutz, G.J. Kunde, W.D. Kunze, V. Lindenstruth, U. Lynen, A. Moroni, W.F.J. Müller, C.A. Ogilvie, J. Pochodzalla, G. Raciti, Th. Rubehn, H. Sann, A. Schüttauf, W. Seidel, W. Trautmann, and A. Wörner, Nucl. Phys. A584 (1995) 737

[11] J.B. Garcia and C. Cerruti, Nucl. Phys. A578 (1994) 597

[12] R. Botet and M. Ploszajczak, Phys. Lett. B312 (1993) 30; Acta Physica Polonica B25 (1994) 353

[13] S. Leray and S. Souza, Proceedings of Second European Biennial Conference on Nuclear Physics, Megève 1993, edited by D. Guinet (World Scientific, Singapore, 1995) p. 81

[14] B. Elattari, J. Richert, P. Wagner, and Y.M. Zheng, Phys. Lett. B356 (1995) 181; Nucl. Phys. A592 (1995) 385

[15] For a recent review see L.G. Moretto and G.J. Wozniak, Ann. Rev. Nucl. Part. Science 43 (1993) 379

[16] M.L. Gilkes, S. Albergo, F. Bieser, F.P. Brady, Z. Caccia, D.A. Cebra, A.D. Chacon, J.L. Chance, Y. Choi, S. Costa, J.B. Elliott, J.A. Hauger, A.S. Hirsch, E.L. Hjort, A. Insolia, M. Justice, D. Keane, J.C. Kintner, V. Lindenstruth, M.A. Lisa, U. Lynen, H.S. Matis, M. McMahan, C. McParland, W.F.J. Müller, D.L. Olson, M.D. Partlan, N.T. Porile, R. Potenza, G. Rai, J. Rasmussen, H.G. Ritter, J. Romanski, J.L. Romero, G.V. Russo, H. Sann, R. Scharenberg, A. Scott, Y. Shao, B.K. Srivastava, T.J.M. Symons, M. Tincknell, C. Tuvé, S. Wang, P. Warren, H.H. Wieman, and K. Wolf, Phys. Rev. Lett. 73 (1994) 1590

[17] J. Pochodzalla, T. Möhlenkamp, T. Rubehn, A. Schüttauf, A. Wörner, E. Zude, M. Begemann–Blaich, Th. Blaich, H. Emling, A. Ferrero, C. Groß, G. Imme, I. Iori, G.J. Kunde, W.D. Kunze, V. Lindenstruth, U. Lynen, A. Moroni, W.F.J. Müller, B. Ocker, G. Raciti, H. Sann, C. Schwarz, W. Seidel, V. Serfling, J. Stroth, W. Trautmann, A. Trzcinski, A. Tucholski, G. Verde, and B. Zwieglinski, Phys. Rev. Lett. 75 (1995) 1040

[18] Th. Rubehn, W.F.J. Müller, R. Bassini, M. Begemann–Blaich, Th. Blaich, A. Ferrero, C. Groß, G. Imme, I. Iori, G.J. Kunde, W.D. Kunze, V. Lindenstruth, U. Lynen, T. Möhlenkamp, L.G. Moretto, B. Ocker, J. Pochodzalla, G. Raciti, S. Reito, H. Sann, A. Schüttauf, W. Seidel, V. Serfling, W. Trautmann, A. Trzcinski, G. Verde, A. Wörner, E. Zude, and B. Zwieglinski, Z. Phys. A 353 (1995) 197

[19] Th. Rubehn, R. Bassini, M. Begemann–Blaich, Th. Blaich, A. Ferrero, C. Groß, G. Imme, I. Iori, G.J. Kunde, W.D. Kunze, V. Lindenstruth, U. Lynen, T. Möhlenkamp, L.G. Moretto, W.F.J. Müller, B. Ocker, J. Pochodzalla, G. Raciti, S. Reito, H. Sann, A. Schüttauf, W. Seidel, V. Serfling, W. Trautmann, A. Trzcinski, G. Verde, A. Wörner, E. Zude, and B. Zwieglinski, Phys. Rev. C53 (1996) 993

[20] Th. Rubehn, R. Bassini, M. Begemann–Blaich, Th. Blaich, A. Ferrero, C. Groß, G. Imme, I. Iori, G.J. Kunde, W.D. Kunze, V. Lindenstruth, U. Lynen, T. Möhlenkamp, L.G. Moretto, W.F.J. Müller, B. Ocker, J. Pochodzalla, G. Raciti, S. Reito, H. Sann, A. Schüttauf, W. Seidel, V. Serfling, W. Trautmann, A. Trzcinski, G. Verde, A. Wörner, E. Zude, and B. Zwieglinski, Phys. Rev. C53 (1996) 3143

[21] W. Trautmann *et al.*, Proceedings of the XXXIII International Winter Meeting on Nuclear Physics, Bormio, 1995, edited by I. Iori (Ricerca Scientifica ed Educazione Permanente, Milano, 1995) p. 372

[22] R.T. De Souza, N. Carlin, Y.D. Kim, J. Ottarson, L. Phair, D.R. Bowman, C.K. Gelbke, W.G. Gong, W.G. Lynch, R.A. Pelak, T. Peterson, G. Poggi, M.B. Tsang, and H.M. Xu, Nucl. Instrum. Methods Phys. Res. A295 (1990) 109

[23] M.B. Tsang, W.C. Hsi, W.G. Lynch, D.R. Bowman, C.K. Gelbke, M.A. Lisa, G.F. Peaslee, G.J. Kunde, M.L. Begemann–Blaich, T. Hofmann, J. Hubele, J. Kempter, P. Kreutz, W.D. Kunze, V. Lindenstruth, U. Lynen, M. Mang, W.F.J. Müller, M. Neumann, B. Ocker, C.A. Ogilvie, J. Pochodzalla, F. Rosenberger, H. Sann, A. Schüttauf, V. Serfling, J. Stroth, W. Trautmann, A. Tucholski, A. Wörner, E. Zude, B. Zwieglinski, S. Aiello, G. Imme, V. Pappalardo, G. Raciti, R.J. Charity, L.G. Sobotka, I. Iori, A. Moroni, R. Scardaoni, A. Ferrero, W. Seidel, Th. Blaich, L. Stuttge, A. Cosmo, W.A. Friedman, and G. Peilert, Phys. Rev. Lett. 71 (1993) 1502

[24] W. Reisdorf *et al.*, Proceedings of the International Workshop XXII, Hirschegg, 1994, edited by H. Feldmeier and W. Nörenberg (GSI, Darmstadt, 1994) p. 93

[25] K. Sümmerer, W. Brüchle, D.J. Morrissey, M. Schädel, B. Szweryn, and Yang Weifan, Phys. Rev. C42 (1990) 2546

[26] V. Lindenstruth, PhD thesis, Universität Frankfurt, 1993, report GSI-93-18

[27] G.J. Kunde, J. Pochodzalla, J. Aichelin, E. Berdermann, B. Berthier, C. Cerruti, C.K. Gelbke, J. Hubele, P. Kreutz, S. Leray, R. Lucas, U. Lynen, U. Milkau, W.F.J. Müller, C. Ngô, C.H. Pinkenburg, G. Raciti, H. Sann, and W. Trautmann, Phys. Lett. B272 (1991) 202

[28] H.W. Barz, H. Schulz, and G.F. Bertsch, Phys. Lett. B217 (1989) 397

[29] D.H. Boal, J.N. Glosli, and C. Wicentowich, Phys. Rev. Lett. 62 (1989) 737

[30] H.W. Barz, J.P. Bondorf, R. Donangelo, H. Schulz, and K. Sneppen, Phys. Lett. B228 (1989) 453

[31] W. Bauer, Phys. Rev. C51 (1995) 803

[32] A.S. Goldhaber, Phys. Lett. 53B (1974) 306

[33] U. Milkau, M.L. Begemann–Blaich, E.-M. Eckert, G. Imme, P. Kreutz, A. Kühmichel, M. Lattuada, U. Lynen, C. Mazur, W.F.J. Müller, J.B. Natowitz, C. Ngô, J. Pochodzalla, G. Raciti, M. Ribrag, H. Sann, W. Trautmann, and R. Trockel, Z. Phys. A346 (1993) 227

[34] A.S. Botvina and D.H.E. Gross, Phys. Lett. B344 (1995) 6; Nucl. Phys. A592 (1995) 257

[35] G.J. Kunde, W.C. Hsi, W.D. Kunze, A. Schüttauf, A. Wörner, M. Begemann–Blaich, Th. Blaich, D.R. Bowman, R.J. Charity, A. Cosmo, A. Ferrero, C.K. Gelbke, J. Hubele, G. Imme, I. Iori, P. Kreutz, V. Lindenstruth, M.A. Lisa, W.G. Lynch, U. Lynen, M. Mang, T. Möhlenkamp, A. Moroni, W.F.J. Müller, M. Neumann, B. Ocker, C.A. Ogilvie, G.F. Peaslee, J. Pochodzalla, G. Raciti, T. Rubehn, H. Sann, W. Seidel, V. Serfling, L.G. Sobotka, J. Stroth, L. Stuttge, S. Tomasevic, W. Trautmann,

M.B. Tsang, A. Tucholski, G. Verde, C.W. Williams, E. Zude, and B. Zwieglinski, Phys. Rev. Lett. 74 (1995) 38

[36] C.J. Waddington and P.S. Freier, Phys. Rev. C31 (1985) 888

[37] V. Lips, R. Barth, H. Oeschler, S.P. Avdeyev, V.A. Karnaukhov, W.D. Kuznetsov, L.A. Petrov, O.V. Bochkarev, L.V. Chulkov, E.A. Kuzmin, W. Karcz, W. Neubert, and E. Norbeck, Phys. Rev. Lett. 72 (1994) 1604

[38] K. Kwiatkowski, K.B. Morley, E. Renshaw Foxford, D.S. Bracken, V.E. Viola, N.R. Yoder, R. Legrain, E.C. Pollacco, C. Volant, W.A. Friedman, R.G. Korteling, J. Brzychczyk, and H. Breuer, Phys. Rev. Lett. 74 (1995) 3756

[39] G. Rusch, W. Heinrich, B. Wiegel, E. Winkel, and J. Dreute, Phys. Rev. C49 (1994) 901

[40] P.L. Jain and G. Singh, Phys. Rev. C46 (1992) R10

[41] P.L. Jain, G. Singh, and A. Mukhopadhyay, Phys. Rev. C50 (1994) 1085

[42] M.L. Cherry, A. Dabrowska, P. Deines-Jones, A.J. Dubinina, R. Holynski, W.V. Jones, E.D. Kolganova, A. Olszewski, E.A. Pozharova, K. Sengupta, T.Yu. Skorodko, V.A. Smirnitski, M. Szarska, C.J. Waddington, J.P. Wefel, B. Wilczynska, and W. Wolter, Z. Phys. C 63 (1994) 549

[43] M.L. Cherry, A. Dabrowska, P. Deines-Jones, R. Holynski, W.V. Jones, E.D. Kolganova, A. Olszewski, K. Sengupta, T.Yu. Skorodko, M. Szarska, C.J. Waddington, J.P. Wefel, B. Wilczynska, B. Wosiek, and W. Wolter, Phys. Rev. C 52 (1995) 2652

[44] G.F. Peaslee, M.B. Tsang, C. Schwarz, M.J. Huang, W.S. Huang, W.C. Hsi, C. Williams, W. Bauer, D.R. Bowman, M. Chartier, J. Dinius, C.K. Gelbke, T. Glasmacher, D.O. Handzy, M.A. Lisa, W.G. Lynch, C.M. Mader, L. Phair, M-C. Lemaire, S.R. Souza, G. Van Buren, R.J. Charity, L.G. Sobotka, G.J. Kunde, U. Lynen, J. Pochodzalla, H. Sann, W. Trautmann, D. Fox, R.T. de Souza, G. Peilert, W.A. Friedman, and N. Carlin, Phys. Rev. C49 (1994) R2271

[45] L. Pienkowski, H.G. Bohlen, J. Cugnon, H. Fuchs, J. Galin, B. Gatty, B. Gebauer, D. Guerreau, D. Hilscher, D. Jacquet, U. Jahnke, M. Josset, X. Ledoux, S. Leray, B. Lott, M. Morjean, A. Péghaire, G. Röschert, H. Rossner, R.H. Siemssen, and C. Stéphan, Phys. Lett. B336 (1994) 147

[46] J. Dreute, W. Heinrich, G. Rusch, and B. Wiegel, Phys. Rev. C44 (1991) 1057

[47] S.B. Kaufman and E.P. Steinberg, Phys. Rev. C22 (1980) 167

[48] R.E.L. Green and R.G. Korteling, Phys. Rev. C22 (1980) 1594

[49] N.T. Porile, A.J. Bujak, D.D. Carmony, Y.H. Chung, L.J. Gutay, A.S. Hirsch, M. Mahi, G.L. Paderewski, T.C. Sangster, R.P. Scharenberg, and B.C. Stringfellow, Phys. Rev. C39 (1989) 1914

[50] B. Berthier, R. Boisgard, J. Julien, J.M. Hisleur, R. Lucas, C. Mazur, C. Ngô, M. Ribrag, and C. Cerruti, Phys. Lett. B193 (1987) 417

[51] W. Trautmann, U. Milkau, U. Lynen, and J. Pochodzalla, Z. Phys. A 344 (1993) 447

[52] J.-J. Gaimard and K.-H. Schmidt, Nucl. Phys. A531 (1991) 709

[53] K.-H. Schmidt, T. Brohm, H.-G. Clerc, M. Dornik, M. Fauerbach, H. Geissel, A. Grewe, E. Hanelt, A. Junghans, A. Magel, W. Morawek, G. Münzenberg, F. Nickel, M. Pfützner, C. Scheidenberger, K. Sümmerer, D. Vieira, B. Voss, and C. Ziegler, Phys. Lett. B300 (1993) 313;
T. Brohm and K.-H. Schmidt, Nucl. Phys. A569 (1994) 821

[54] Z. Koba, H.B. Nielsen, and P. Olesen, Nucl. Phys. B40 (1972) 317

[55] For a recent review see Ziping Chen, Int. J. Mod. Phys. E2 (1993) 285

[56] Y. Yariv and Z. Fraenkel, Phys. Rev. C20 (1979) 2227; Phys. Rev. C24 (1981) 488

[57] J. Cugnon, Nucl. Phys. A462 (1987) 751

[58] G.E. Brown, Nucl. Phys. A488 (1988) 689c

[59] K. Kwiatkowski, W.A. Friedman, L.W. Woo, V.E. Viola, E.C. Pollacco, C. Volant, and S.J. Yennello, Phys. Rev. C49 (1994) 1516

[60] J.W. Harris, G. Odyniec, H.G. Pugh, L.S. Schroeder, M.L. Tincknell, W. Rauch, R. Stock, R. Bock, R. Brockmann, A. Sandoval, H. Ströbele, R.E. Renfordt, D. Schall, D. Bangert, J.P. Sullivan, K.L. Wolf, A. Dacal, C. Guerra, and M.E. Ortiz, Phys. Rev. Lett. 58 (1987) 463

[61] C. Müntz, P. Baltes, H. Oeschler, A. Sartorius, A. Wagner, W. Ahner, R. Barth, M. Cieślak, M. Debowski, E. Grosse, W. Henning, P. Koczoń, D. Miśkowiec, R. Schicker, P. Senger, C. Bormann, D. Brill, Y. Shin, J. Stein, R. Stock, H. Ströbele, B. Kohlmeyer, H. Pöppl, F. Pühlhofer, J. Speer, K. Völkel, and W. Walus, Z. Phys. A352 (1995) 175, and references therein

[62] V.S. Barashenkov and V.D. Toneev, Interactions of high-energy particles and atomic nuclei with nuclei, Moscow, Atomizdat, 1972 (in Russian);
V.D. Toneev, private communication (1994)

[63] D.H.E. Gross, Rep. Prog. Phys. 53 (1990) 605;
A.R. DeAngelis and D.H.E. Gross, Comput. Phys. Commun. 76 (1993) 113

[64] W.A. Friedman, Phys. Rev. C42 (1990) 667

[65] G. Papp and W. Nörenberg, preprint GSI-95-30 (1995)

[66] W. Bauer, private communication (1991)

[67] P. Désesquelles, J.P. Bondorf, I.N. Mishustin, and A.S. Botvina, Nucl. Phys. A, in print

[68] P. Désesquelles, private communication (1996)

[69] A.S. Botvina and Hongfei Xi, private communication (1996)

[70] X. Campi, H. Krivine, and E. Plagnol, Phys. Rev. C50 (1994) R2680